A REVERSIBLE NUCLEAR RADIATION APPROACH TO GENERATION-RECOMBINATION NOISE STUDIES IN GE-SINGLE CRYSTALS

By

ED RAYMOND McCARTER

Bachelor of Science
Oklahoma State University
Stillwater, Oklahoma
1951

Master of Science
Oklahoma State University
Stillwater, Oklahoma
1965

Submitted to the faculty of the Graduate College
of the Oklahoma State University
in partial fulfillment of the requirements
for the degree of
DOCTOR OF PHILOSOPHY
May, 1967

A REVERSIBLE NUCLEAR RADIATION APPROACH

TO GENERATION-RECOMBINATION NOISE

STUDIES IN GE-SINGLE CRYSTALS

Thesis Approved:

Hans R Bilger
Thesis Adviser

William J. Lewis

Wm. L. Hughes

D D Durham
Dean of the Graduate College

ACKNOWLEDGMENTS

My most sincere gratitude goes to my thesis adviser, Professor Hans R. Bilger, for his encouragement, valuable comments, and aid throughout my doctoral studies. I am especially indebted to him for the original idea of this thesis and the very excellent guidance throughout my research.

I also wish to thank the other members of my graduate committee, Professors W. L. Hughes and W. J. Leivo, for their advice and encouragement, and Professor Jeanne L. Agnew who graciously served during the early portion of my research.

The help of the Radiation Laboratory of the Continental Oil Company is gratefully acknowledged in providing the gamma irradiation.

The Radiation Laboratory of Phillips Petroleum Company is also gratefully appreciated in providing the neutron irradiation.

Finally, I wish to express my gratitude to Esso Production Research Company for financial support which made my studies possible and to my wife, Becky, for her understanding and encouragement throughout my studies.

TABLE OF CONTENTS

Chapter Page

LIST OF TABLES

LIST OF FIGURES

Figure Page

CHAPTER I

INTRODUCTION

1.1 Statement of the Problem. In the early part of this century, the work on noise was mainly theoretical. Schottky (23) in 1918 first reported the shot effect found in temperature-limited vacuum diodes caused by the plate current fluctuations. Fluctuations of the voltage across a resistor due to the thermal motion of the electrons were discovered by Nyquist (20) in 1928. Four years later in 1932, Williams and Thatcher (34) reported noise in excess of thermal noise. Bernamont (1) made a thorough study of this type of noise in 1937 where he found a power spectrum of the type 1/f. As semiconductor crystals became available, much work went into the theoretical and applied aspects of these crystals. In 1951, Herzog and van der Ziel (13) were the first to report a spectrum of the type $C/(1 + f^2 \tau^2)$ for germanium single crystals. As discussed in Chapter II, Burgess (3, 4, 5) in 1954 provided the theory for the magnitude of the mean square fluctuations; and two years later, van Vliet and Blok (32) extended the theory to include the frequency dependence and introduced the term, generation-recombination (g-r) noise. Today, the entire history and theories of g-r noise are well summarized (6, 15, 17, 26, 29, 30, 31); and much of the theory has been verified by experimental evidence (6). In this thesis, a unique tool is developed for testing some of the features of g-r noise. The lifetime and apparent doping may be varied in a

controlled and reversible manner. For example, the lifetime was varied by a factor of 10^3; and the crystal changed from n to p and back to n.

Secondly, a new type of noise spectrum has been found in gamma-irradiated crystals which is not explainable by the older theories and should open the door for further refinement in the noise theory of semiconductors with traps and recombination centers.

1.2 Scope of Investigation. With the use of monoenergetic 14.7 MeV neutrons and ^{60}Co gamma rays, variations in the lifetime of a germanium single crystal of up to 10^3 and apparent doping changes from n type to p type have been accomplished. As can be seen from the theory in Chapter II, these are the most important parameters in the g-r noise theory. By annealing, these changes have been reversed so that the original properties of the crystal are once more obtained. The methods used in this process are such that 1/f type noise has been virtually eliminated from the noise studies (in the frequency range used, 20 Hz to 1.5 MHz). The crystal dimensions and surface properties remain the same through the experiment within the measurement capabilities.

Noise measurement techniques for determining the spectra have been used for measuring noise at very low amplitudes with an amplifier whose R_{eq} is 95 ohms (this corresponds to 0.04 μV in a bandwidth of 1 KHz) and with good accuracy using a wave analyzer with only a 6.75 Hz bandwidth (see Appendix A). Spectra with a $1/(1 + \omega^2 \tau^2)$ dependence have been obtained in germanium single crystals with cutoff frequencies $\left(S_i \text{ (f cutoff)}/S_i \text{ (f} \rightarrow 0) = 1/2\right)$ down to 88 Hz which, to the author's knowledge, is the lowest reported to date. The details of these methods

are given in Chapter III.

Further confirmation of the g-r noise theory is given by the experimental results discussed in Chapter IV. In addition, spectra are presented which indicate a resonance effect occurring in a gamma-irradiated p-type crystal. This effect is not explainable by either the present g-r noise theory or the theory of ambipolar drift. An explanation of this effect has not been attempted, but it probably will have to make use of the fact that irradiation creates recombination centers with a multiple level structure in the forbidden band with overlapping wave functions.

CHAPTER II

THEORY OF GENERATION-RECOMBINATION NOISE IN A SEMICONDUCTOR

2.1 Introduction. A treatment of g-r noise with three and more reservoirs of electrons and holes (levels), based on the theory of stationary Markoffian processes, has been given by van Vliet (30) and van der Ziel (26). Since no original work on the theory of g-r noise is presented in this thesis, only an outline of the pertinent aspects of g-r noise is given, together with the underlying assumptions:

(a) The noise is not necessarily Gaussian.

(b) The fluctuations are from a non-equilibrium, steady-state value (n_o).

(c) The system is linear; i.e., its responses to external forces are linear in these forces.

A critical examination can be found in Chapter VII of Burgess (6).

2.2 Method of Solving Markoff Random Processes. We will now consider the fluctuations caused by generation and recombination of electrons and holes in a semiconductor with recombination centers at a single energy level lying in the forbidden band as shown in Figure 2.2.1.

Let the rate of generation be g(n) when there are n carriers in the conduction band and the rate of recombination be r(n). For a near

intrinsic n-type semiconductor with N_D donors, we will take with Burgess (3, 4, 5):

$$g(n) = \gamma \qquad r(n) = \delta pn \tag{2.2.1}$$

where γ and δ are constants. Burgess (3, 4, 5) was the first to find the mean square fluctuation:

$$< \Delta n^2 > = \frac{n_o p_o}{n_o + p_o} \tag{2.2.2}$$

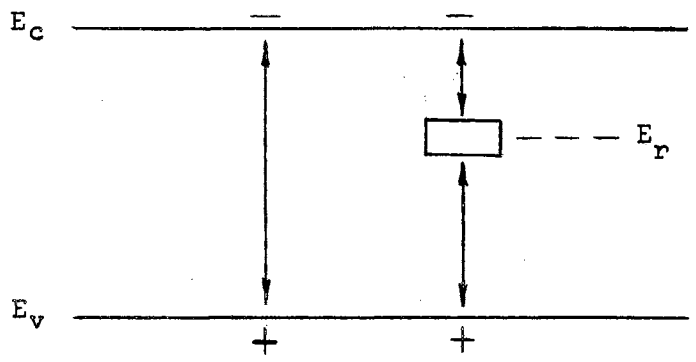

Figure 2.2.1. Semiconductor Forbidden Band With Recombination Center

If the concentration of one type of carrier is very small, then we have either $< \Delta n^2 > = n_o$ or $< \Delta n^2 > = p_o$, which is the fluctuation of a Poisson distribution (implies independence of events). Lax (18, 19) shows that the distribution in lifetimes results in an exponential decay of the carrier concentration as given by:

$$< \Delta n(t) > = \Delta n_o \exp - t/\tau \tag{2.2.3}$$

where $\Delta n(t)$ is the fluctuation at time t and Δn_o is the fluctuation at

time t = 0. The autocorrelation function follows as

$$< \Delta n(t)\ \Delta n_o > = < \Delta n^2 > \exp - t/\tau \qquad (2.2.4)$$

The important Wiener-Khintchine theorem can then be applied to the correlation function to obtain the spectral density as follows:

$$S(f) = 4 \int_o^\infty < \Delta n(t)\ \Delta n_o > \cos(\omega t)\ dt \qquad (2.2.5)$$

which results in

$$S(f) = 4 \frac{n_o\ p_o}{n_o + p_o} \cdot \frac{\tau}{1 + (\omega\tau)^2} \qquad (2.2.6)$$

Van Roosbroeck and Shockley (28) have found that the direct transitions between the valence and conduction band result in lifetimes > 100 ms in Ge at room temperatures. These are never found in practice because of lattice imperfections.

If one of the two transitions involving the recombination center results in a much larger τ than the other transition, then a simple g-r spectrum follows (see van Vliet (29)) where the τ happens to be the Shockley-Read lifetime.

One can readily convert Equation 2.2.6 to $S_i(I)$, the spectral density of the current noise, by noting that

$$I_{dc} = (q\ \mu_n\ n_o + q\ \mu_p\ p_o) \frac{E}{L} \qquad (2.2.7)$$

The fluctuation of the current follows as

$$< \Delta i^2 > = q^2\ \mu_p^2\ (1 + b)^2 < \Delta n_o^2 > \frac{E^2}{L^2} \qquad (2.2.8)$$

where $b = \mu_n/\mu_p$ and where we have used the fact that $\Delta n_o = \Delta p_o$. Applying Equations 2.2.7 and 2.2.8 to the Wiener-Khintchine theorem, Equation 2.2.5 results in

$$S_i(I) = 4\, I_{dc}^2 \cdot \frac{(b+1)^2}{(bn_o + p_o)^2} \cdot \frac{n_o\, p_o}{n_o + p_o} \cdot \frac{\tau}{1 + (\omega\tau)^2} \qquad (2.2.9)$$

The spectral density of the thermal noise $S_i(R)$ or Nyquist (20) noise, as it is often called, is given as

$$S_i(R) = \frac{4\, kT}{R} \qquad (2.2.10)$$

By applying the principle of detailed balance ($np = n_i^2$) and the Einstein relation $D = \mu kT/q$ in conjunction with Equations 2.2.9 and 2.2.10, we can readily arrive at the noise ratio n_r as given in Equation 2.2.11:

$$n_r = \frac{S_i(I)}{S_i(R)} = \left(\frac{b+1}{q\, W_d}\right)^2 \cdot \frac{I_{dc}^2}{D_p} \cdot \frac{n_i^2}{(bn + p)^3\,(n + p)} \cdot \frac{\tau}{1 + (\omega\tau)^2} \qquad (2.2.11)$$

where

$S_i(I)$ = spectral density of current noise (A^2s)

$S_i(R)$ = spectral density of thermal noise (A^2s)

$b = \mu_n/\mu_p$ = ratio of electron and hole mobilities

q = electron charge (1.6×10^{-19} As)

W_d = cross section of the crystal (m^2)

I_{dc} = direct current through the crystal (A)

D_p = diffusion coefficient of holes (m^2/s)

n_i, n, p = intrinsic, electron, hole concentrations (m^{-3})

τ = Shockley-Read lifetime (s)

The equations in this thesis are always in the MKS system; whereas, for convenience, numbers are sometimes given in other units (τ in μs, mobilities in cm^2/Vs, etc.).

2.3 Multilevel Generation-Recombination. A very elegant treatment to multilevel g-r noise using a thermodynamic approach has been given by van Vliet (29). Figure 2.3.1 illustrates the energy level distribution under consideration.

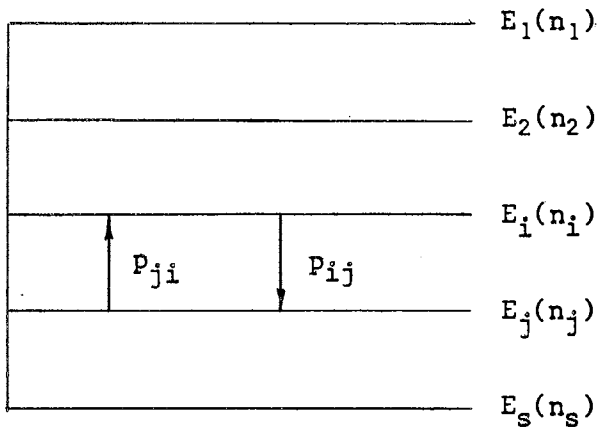

P_{ij} = transition probabilities (sec^{-1})

$E_k(m_k)$ = k-th energy level with a concentration of electrons = n_k

Figure 2.3.1. Multilevel Energy Distribution

The variances of the carrier fluctuations (α) are given by the generalized g-r theorem as

$$\underline{a} < \underline{\alpha}\,\underline{\alpha} > + < \underline{\alpha}\,\underline{\alpha} > \underline{a}^{T} = - \underline{B} \qquad (2.3.1)$$

where $< \underline{\alpha}\,\underline{\alpha} >$ is the matrix with elements $< \alpha_i\, \alpha_j >$. The elements of matrix $\underline{a}$ are given by

$$a_{i\ell} = \sum_{\substack{j=1 \\ j \neq j}}^{s} (\partial\, p_{ij}/\partial\, \alpha_\ell - \partial\, p_{ij}/\partial\, \alpha_\ell)_o \qquad (2.3.2)$$

and the elements of matrix $\underline{B}$ are given by

$$B_{ii} = 2 \sum_{\substack{k=1 \\ k \neq i}}^{s} p^o_{ik} \qquad (2.3.3)$$

$$B_{ij} = - p^o_{ij} - p^o_{ji} \qquad (i \neq j) \qquad (2.3.4)$$

The superscript o means the equilibrium rates. A matrix $\underline{C}$ is then found which diagonalizes $\underline{a}$ with the eigenvalues of $\underline{a}$ being the elements of the diagonal matrix $\tau_k^{-1}\, \underline{I}$. The spectral density is then given by

$$G_{mn} = 4 \sum_{k=1}^{s=1} \sum_{i \neq n}^{s} (c^{-1})_{mk}\, p^o_{in}\, (c_{kn} - c_{ki})\, \tau_k^2/(1 + \omega^2\, \tau_k^2) \qquad (2.3.5)$$

From this it can be seen that the resultant spectra will always be relatively smooth with no peaks or resonances.

In this derivation, the α's are taken as independent (no interaction with each other). It should be noted that interacting levels in the forbidden zone could produce something totally different from the relatively smooth superposition of simple g-r spectra. Taking the special case for a semiconductor with only one recombination center and letting the direct transitions between valence and conduction bands have very low probability so that they may be neglected (which is the actual case in Ge), then Equation 2.3.5 takes the following form for the spectral densities of $< \Delta n^2 >$, $< \Delta p^2 >$, and $< \Delta n\, \Delta p >$:

$$G_{nn} = \sum_{1,2} \frac{4\tau_1^2}{1+\omega^2\tau_1^2} \cdot \frac{\tau_1 (a_{11}\tau_2 + 1) n_o (N - i_o)}{(\tau_1 - \tau_2)\tau_{n_o} N} \qquad (2.3.6)$$

$$G_{pp} = \sum_{1,2} \frac{4\tau_1^2}{1+\omega^2\tau_1^2} \cdot \frac{\tau_2 (a_{11}\tau_1 + 1) p_o i_o}{(\tau_2 - \tau_1)\tau_{p_o} N} \qquad (2.3.7)$$

$$G_{np} = \sum_{1,2} \frac{4\tau_1^2}{1+\omega^2\tau_1^2} \cdot \frac{\tau_1 \tau_2 a_{21} n_o (N - i_o)}{(\tau_2 - \tau_1)\tau_{n_o} N} \qquad (2.3.8)$$

where $\sum_{1,2}$ means that a similar term is added with τ_1 and τ_2 interchanged and i_o is $N (1 + n_1/n_o)^{-1}$ where N is the number of centers.

Figure 2.3.2 shows a calculated example for Gi where

$$G_i = \frac{i^2}{(bn_o + p_o)^2} (b^2 G_{nn} + 2b G_{np} + G_{pp}) \qquad (2.3.9)$$

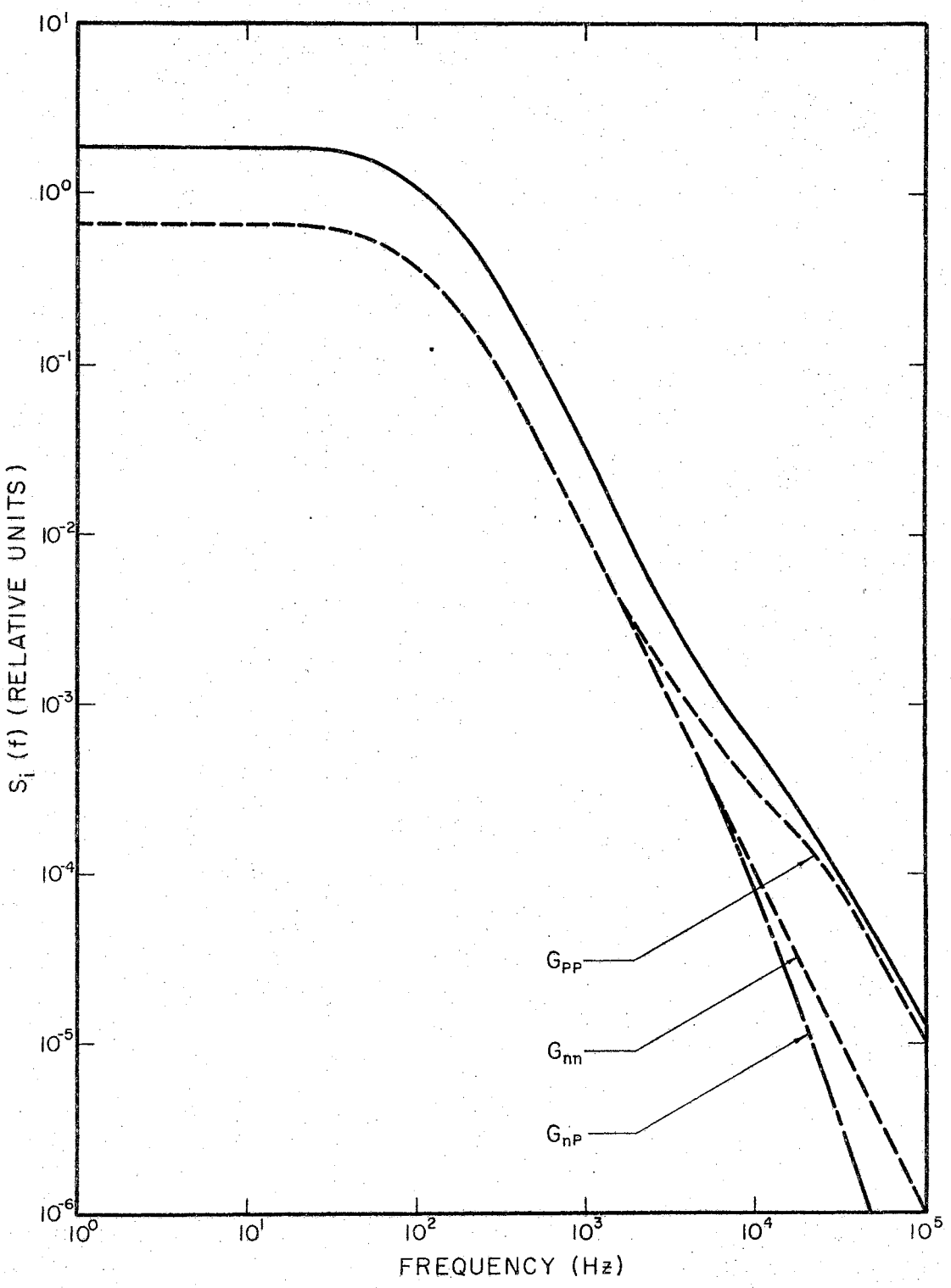

Figure 2.3.2. Theoretical Curve of $S_i(f)$ vs. Frequency for a p-Type Crystal With $N_A = 5 \times 10^{11}$, $n_o = 5 \times 10^{11}$, $p_o = 5 \times 10^{13}$, $\tau_1 = 8.23$ μs, $\tau_2 = 1.26$ ms

CHAPTER III

EXPERIMENTAL ARRANGEMENTS

3.1 General Procedure of the Experiments. The noise signals are generated in a single crystal which is mounted in a thermostatically-controlled chamber. They are amplified and passed through a wave analyzer which selects a narrow frequency range and rectifies the resultant output. The rectified output voltage is displayed on a built-in voltmeter for the 3 KHz to 1.5 MHz wave analyzer, is integrated (see Appendix A), and subsequently displayed on an external voltmeter for the 20 Hz to 50 KHz wave analyzer. A block diagram is outlined in Figure 3.1.1.

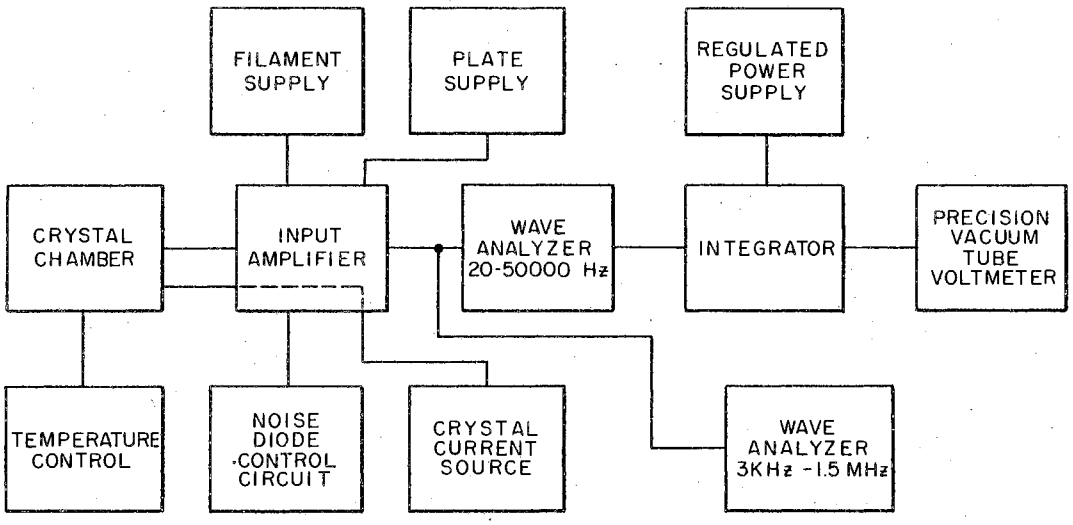

Figure 3.1.1. Block Diagram of Experimental Arrangement for Noise Studies

3.2 Thermostatically-Controlled Chamber. The crystal to be measured is placed in a copper chamber which is well shielded, both electrically and thermally. The temperature of the chamber is sensed by a Fenwall thermal switch which controls the power via a transistorized regulator to a 100-watt heating element located in the chamber. Thermal damping is provided between the heating element and the thermal switch (by partial insulation) to critically damp the system. For cooling, either dry ice or natural ice is placed in the chamber and the temperature controlled with the heating element. The chamber temperature is controlled to $\pm 0.2^{\circ}C$ for temperatures above room temperature and $\pm 0.5^{\circ}C$ for temperatures below room temperature.

The entire copper chamber is suspended in a system (with low mechanical resonance frequency (about 2 Hz)) to prevent external vibrations from affecting the measurements. Figure 3.2.1 shows the amplifier and copper chamber with the suspension system. The DC feeding resistors are placed inside the copper chamber as shown in Figure 3.3.1. A floating power supply is used for the DC crystal current, and the current leads are routed through the amplifier to eliminate external noise pickup.

3.3 Input Amplifier. A common input amplifier is used to drive both the high-frequency and the low-frequency wave analyzer. This amplifier is illustrated in Figure 3.3.1. The first tube is a selected E810F, which is a Phillips (Amperex) tube made in Holland. This tube is capable of operating with a g_m of 50 mA/Volt; but, in order to obtain a good compromise at high and low frequencies, an operating point was chosen which resulted in a g_m of 33 mA/Volt. The theoretical equivalent

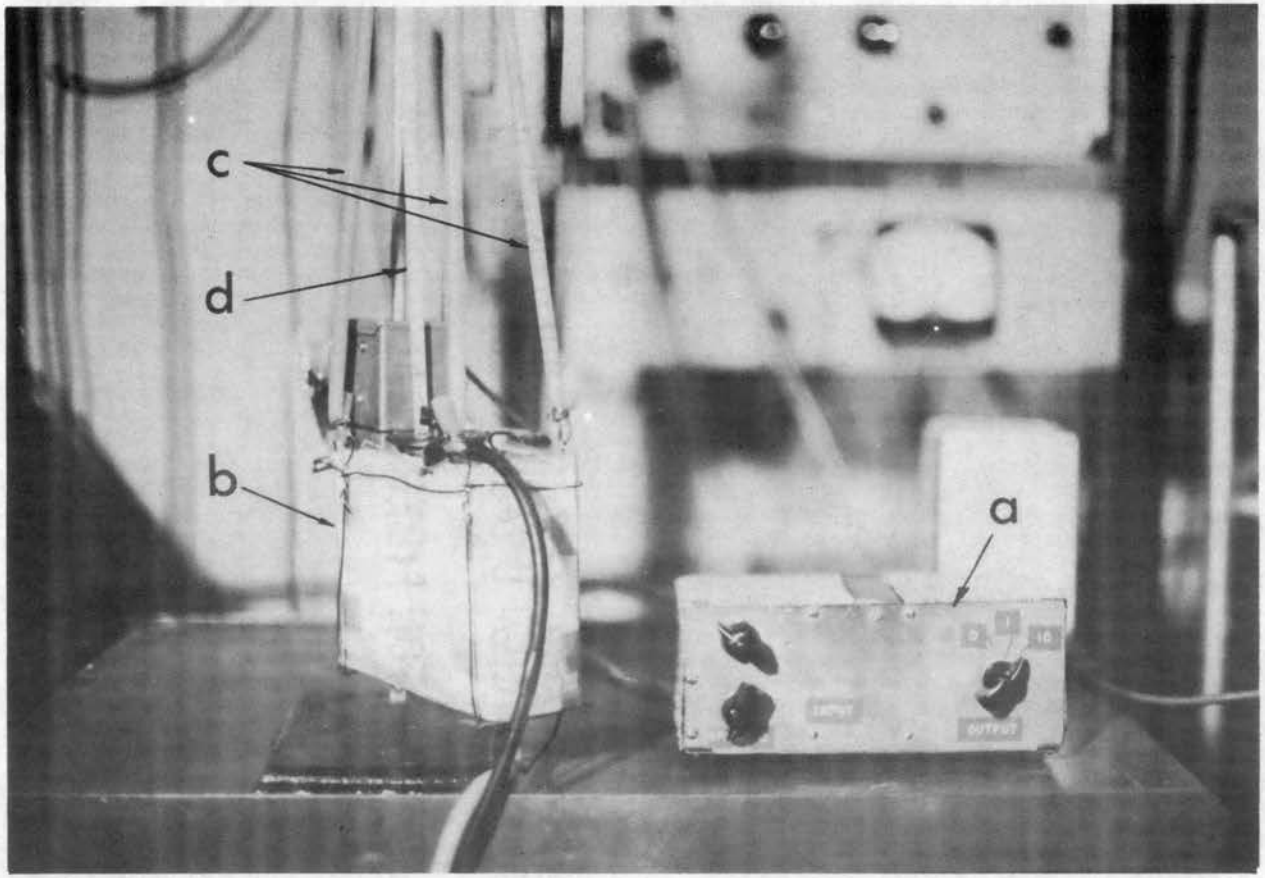

Figure 3.2.1. Amplifier and Suspended Copper Chamber
a. Amplifier c. Suspension Hose
b. Copper Block d. Thermometer

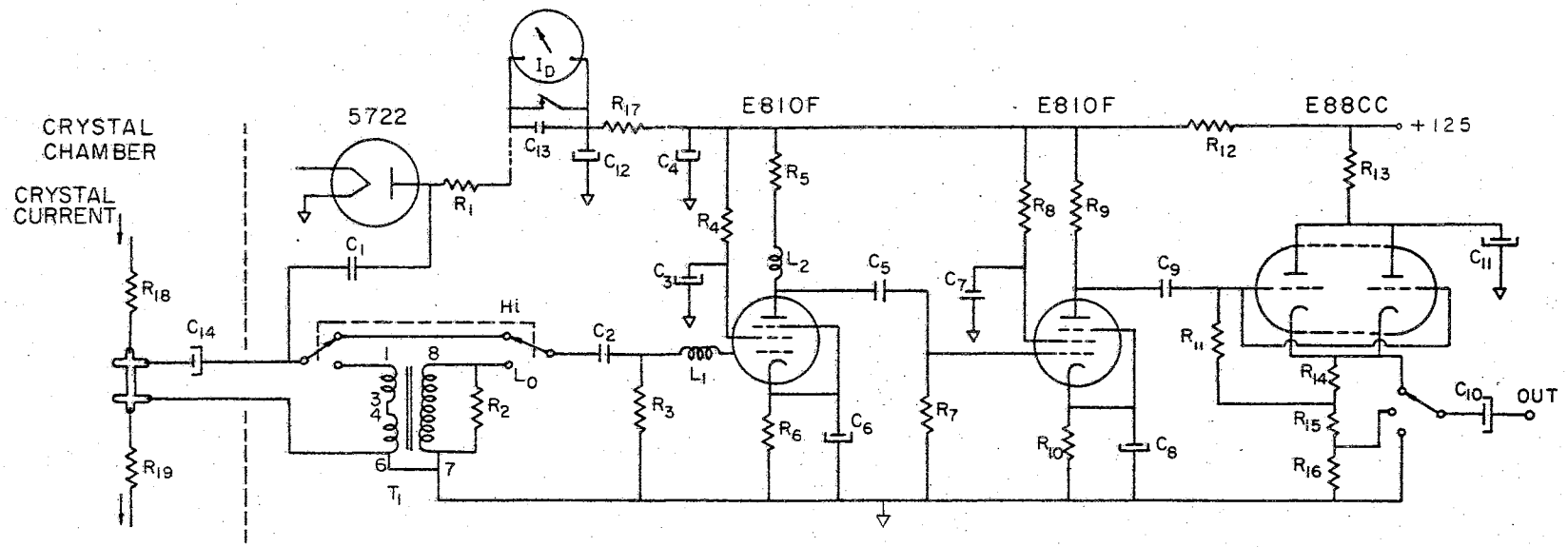

Figure 3.3.1. Input Amplifier and Crystal Chamber Wiring Diagram

noise resistance (R_{eq}) for a pentode is given by Glassford (12) as

$$R_{eq} = \frac{2.5}{g_m}\left(1 + \frac{8\ I_{sg}}{g_m}\right) \qquad (3.3.1)$$

where

I_{sg} = screen grid current, (A)

g_m = transconductance (A/V)

The first tube is operated with an I_{sg} = 1.1 mA which results in a calculated R_{eq} of 104 ohms. By comparing the tube noise with the Nyquist (20) noise

$$V^2 = 4\ kT\ R\ \Delta f \qquad (3.3.2)$$

where

k = Boltzmann's constant (joule/°K)

T = temperature (°K)

R = (equivalent) resistance (ohms)

Δf = effective bandwidth (Hz)

V = RMS voltage referred to input (V)

R_{eq} = 95 ohms was obtained which is close to the calculated value. At lower frequencies, 1/f noise occurs. At 40 Hz, the R_{eq} has increased to 950 ohms.

Metal film and wire-wound resistors are used in the grid, cathode, and plate circuits of the input stage to prevent any excess noise from these elements. A small inductor is connected between the grid and input circuit which prohibits parasitic oscillations in the input stage. A 23.5 μH inductor is connected in series with the plate resistor to increase the overall amplifier bandwidth to 8.5 MHz. The low-frequency

cutoff point is 10 Hz, which is achieved by using large cathode and screen grid bypass capacitors and adequate coupling capacitors.

A second E810F tube increases the gain of the amplifier to 685. An E810F was chosen for this position in the amplifier because of its high g_m. The third tube is an E88CC with both sections paralleled, which doubles the g_m of the stage, and gives a resultant output impedance of 70 ohms. A 10:1 attenuator which is independent of frequency is provided to attenuate large output signals and for test purposes. The third stage is decoupled in the plate supply source from the first two stages, which prevents internal oscillation in the amplifier.

The input circuit is arranged to keep the input impedance as high as possible, which reduces attenuation of the input signals. As noted from Figure 3.3.1, a Hi-Lo switch is provided on the input circuit. The Hi position is R-C coupled to the input tube and is primarily for use when measuring high resistance crystals whose Nyquist noise is greater than or equal to the noise due to the amplifier R_{eq}. For low resistance crystals whose Nyquist noise is less than the noise due to the amplifier R_{eq} (at low frequencies where 1/f noise predominates), a transformer is switched into the input circuit. The amplifier R_{eq} in this mode of operation is then 240 ohms over the frequency range of 20 Hz to 25 KHz. A 20 μF capacitor is provided in the transformer primary circuit which blocks crystal current from the transformer input circuit. The secondary winding of the transformer is damped with a 221 Kohm resistor which makes the transformer gain of 12.8 constant over the above frequency range, excluding the tailing off at the high and low ends of the range.

3.4 Wave Analyzers and Indicating Circuitry. The amplifier output

is connected to two wave analyzers in parallel (HP 310A and HP 302A). The high-frequency analyzer (310A) is usually operated with the 3 KHz bandwidth. The rectified output meter reading is smoothed by an additional 1,000 μF capacitance. The low-frequency analyzer (302A) uses only a 6.75 Hz bandwidth, so the rectified signal is integrated (see Figure 3.4.1 and Appendix A) over 100 seconds and the results read on an accurate DC voltmeter (HP 412A). Figure 3.4.2 shows the complete noise measuring setup.

3.5 Calibration Procedure. The calibration procedure using a temperature limited diode is given by van Vliet (31). In order to insure that the 5722 noise diode acts as it should, q was measured using the following equation (see van der Ziel (27)) for the mean square noise current from a temperature limited diode:

$$\overline{i^2} = 2q\, I_D\, \Delta f \qquad (3.5.1)$$

where

q = charge of an electron (1.602095×10^{-19} As)

I_D = diode plate current (A)

Δf = effective bandwidth of measuring equipment (Hz)

When the 5722 is on, operating at $I_D = 0.9$ mA, the added plate conductance is 1/800 Kohms and the total input capacitance changes by 6.7 pF. This does not affect the measurements. The wave analyzer output is full-wave rectified. A conversion to RMS (see Equation 3.5.1) was calculated and checked, using sine waves. The bandwidth in equation 3.5.1 was evaluated by graphical integration of the measured squared response for a sine input. Using the data as shown in Figure

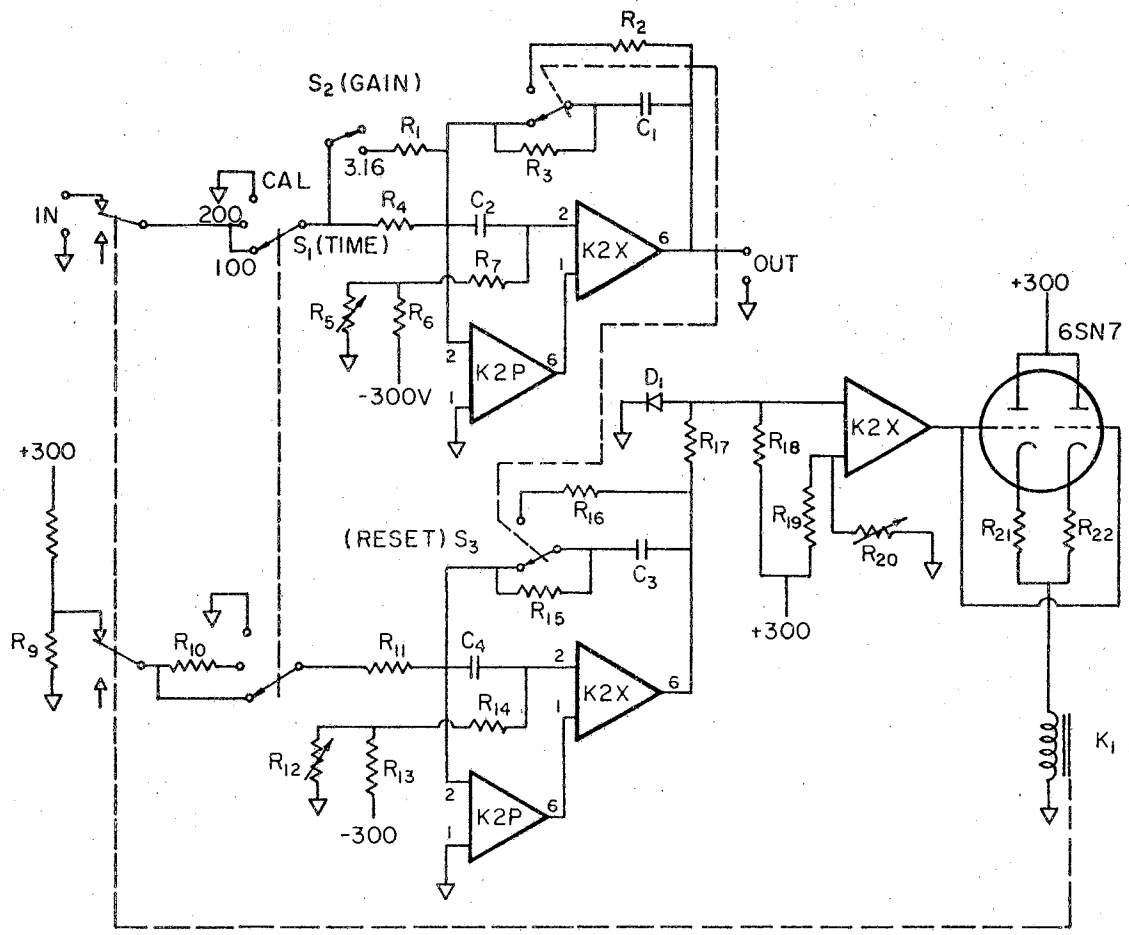

R_1 - 464K	R_8 - 300K	R_{15} - 1M	R_{22} - 470
R_2 - 1K	R_9 - 1K	R_{16} - 1K	D_1 - WE347
R_3 - 1M	R_{10} - 1M	R_{17} - 100K	C_1 - 2μF
R_4 - 1M	R_{11} - 1M	R_{18} - 300K	C_2 - 0.1μF
R_5 - 10K	R_{12} - 10K	R_{19} - 1M	C_3 - 2μF
R_6 - 1M	R_{13} - 1M	R_{20} - 5K	C_4 - 0.1μF
R_7 - 22M	R_{14} - 22M	R_{21} - 470	K_1 - R45A-53913

K2X, K2P - OPERATIONAL AMPLIFIERS (G.A.P.)
PIN 3 - -300V, PIN 4 - GND, PIN 5 - +300V, PIN 7, 8 - HTR.

Figure 3.4.1. Integrator Wiring Diagram

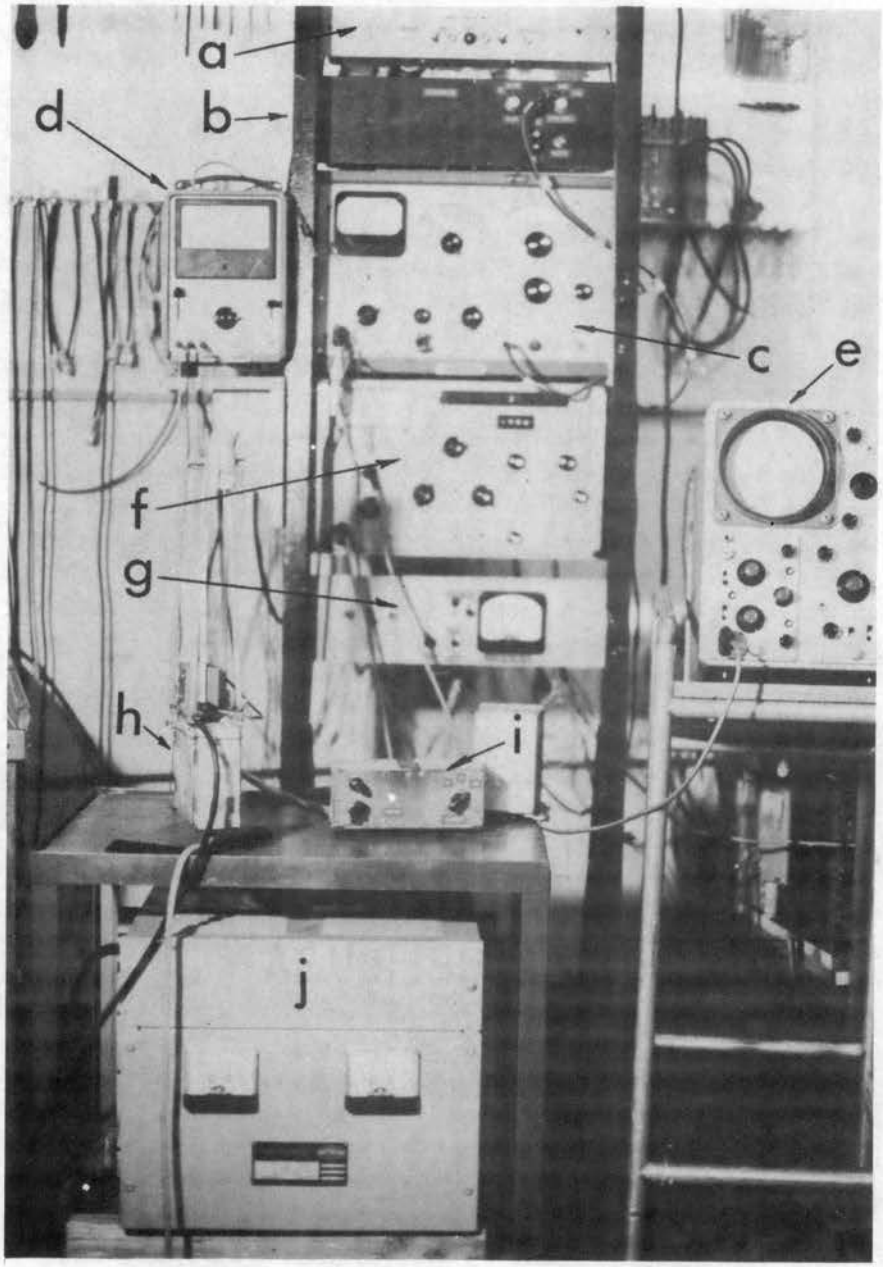

ɟure 3.4.2. Noise Measuring Apparatus

a. Integrator Power Supply
b. Integrator
c. Low-Frequency Wave Analyzer
d. Output VTVM
e. Oscilloscope Monitor
f. High-Frequency Wave Analyzer
g. Control Panel
h. Copper Crystal Chamber
i. Input Amplifier
j. Power Supply for Heating Element

3.5.1, q was measured as

$$q = (1.60 \pm 0.04) \times 10^{-19} \text{ As}$$

A measurement of q was also made at 30 Hz which confirmed the results at 20 KHz. This is in agreement with the results of van Wijngaarden (33) (i.e., the 5722 shows no 1/f noise at 30 Hz).

3.6 Method of Measurements. In these measurements we will be interested in the spectral density $S_i(f)$ of the current passing through a noise object R.

$$S_i(f) = \frac{\overline{i^2}}{\Delta f} \qquad (3.6.2)$$

where $\overline{i^2}$ in Equation 3.6.2 is measured over a bandwidth Δf. According to van Vliet (28), $S_i(f)$ can be evaluated by making three measurements:

1. Measure $\overline{U_1^2}$ with no current flowing through R. (This is the Nyquist noise of both R and the amplifier R_{eq}.)
2. Apply current to R from an external source and make a second measurement $\overline{U_2^2}$.
3. Apply current to the noise diode and obtain a third measurement $\overline{U_3^2}$ with no current flowing through R.

The noise due to the current through R is $\overline{U_2^2} - \overline{U_1^2}$. The noise due to the noise diode is $\overline{U_3^2} - \overline{U_1^2} = 2q\, I_D\, \Delta f\, R^2$. Using these results in Equation 3.6.2 yields the following:

$$S_i(f) = \frac{\overline{U_2^2} - \overline{U_1^2}}{\overline{U_3^2} - \overline{U_1^2}}\, 2q\, I_D \qquad (3.6.3)$$

Another useful quantity is the noise ratio (n_r):

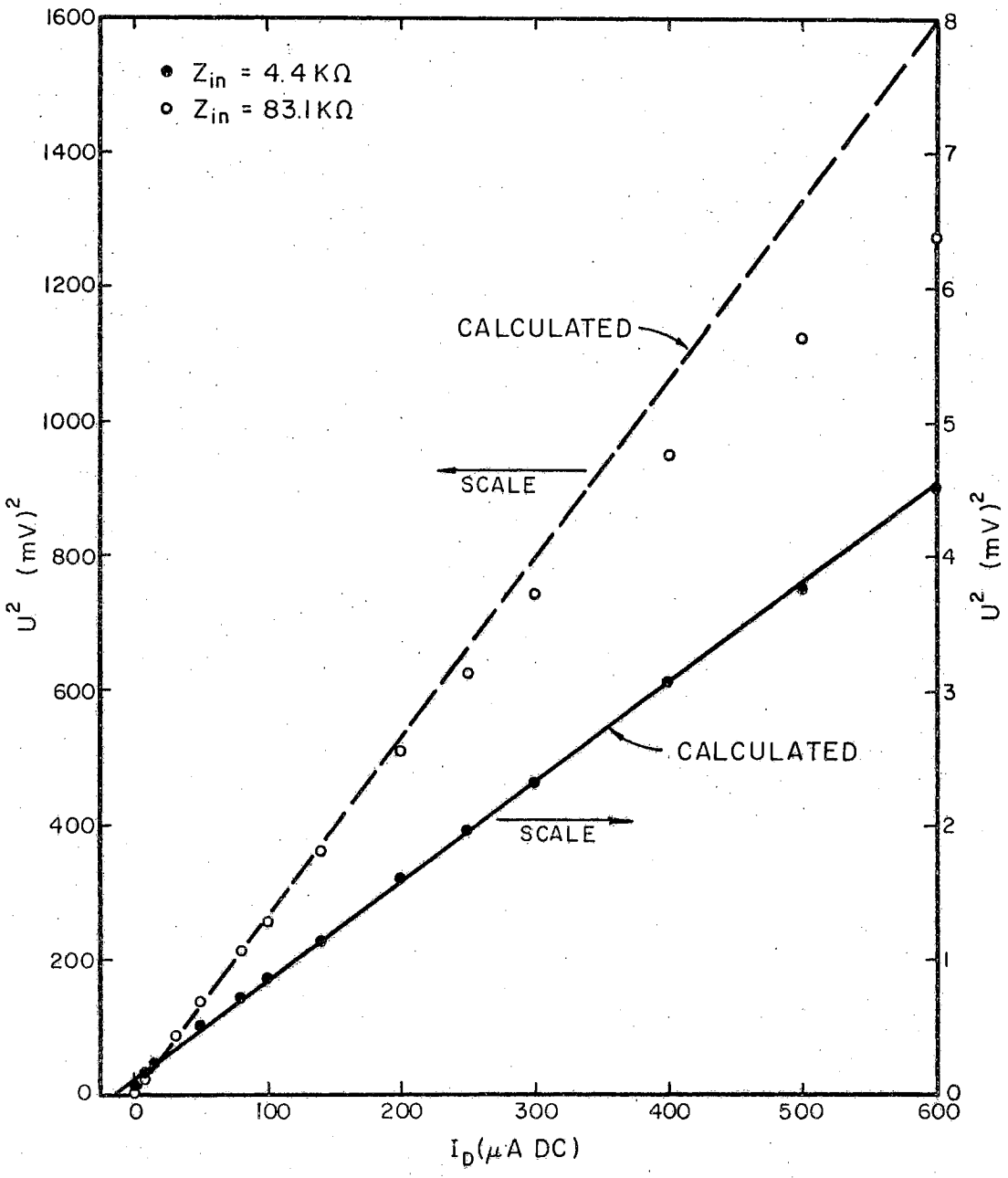

Figure 3.5.1. Mean Square Amplifier Output Voltage Vs. Diode DC Plate Current for 5722 Diode Using High-Frequency Wave Analyzer at 20 KHz

$$n_r = \frac{S_i(f)}{S_i(R)} \qquad (3.6.4)$$

$S_i(R)$ is the spectral density of the noise due to the thermal agitation of the electrons in R. This can be evaluated with the aid of a fourth measurement when R is small ($R < |Z_{in}|/10$) compared to the amplifier input impedance Z_{in}.

4. Short circuit the amplifier input and measure $\overline{U_o^2}$ (this is the noise due to R_{eq}).

The Nyquist noise due to R is then $\overline{U_1^2} - \overline{U_o^2}$. Using this result in Equation 3.6.2 and combining with Equations 3.6.3 and 3.6.4 yields

$$n_r = \frac{\overline{U_2^2} - \overline{U_1^2}}{\overline{U_1^2} - \overline{U_o^2}} \qquad (3.6.5)$$

If R is > $Z_{in}/10$, then an alternate method must be used which entails the direct calculation of $S_i(R)$ as shown by Equation 2.2.10 which can then be used in Equation 3.6.4 to obtain n_r.

3.7 Hall Effect Measurement. In order to determine free carrier-type and concentration, we measure the Hall effect of the crystals. The Hall coefficient R_H, given by (24)

$$E_{Hall} = (J \times B)\, R_H \qquad (3.7.1)$$

where

J = current density (A/m^2)

B = magnetic flux density (Vs/m^2)

E_{Hall} = Hall field intensity (V/m)

is

$$R_H = - \frac{c\,(nb^2 - p)}{q\,(nb + p)^2} \left(\frac{m^3}{As} \right) \qquad (3.7.2)$$

where (16)

$$b = \mu_n/\mu_p = 2.11$$

is used and

$$c = 3\pi/8$$

(Phonon-scattering, see Shockley (24), p. 278).

Figure 3.7.1 shows the experimental arrangement for measuring the Hall effect. The arrangement is essentially an AC bridge (operating frequency $\sim$ 1 KHz) which gives $R_x = R_H \cdot B/d_{eff}$ after balancing (where d_{eff} = effective crystal thickness).

Figure 3.7.2 shows the experimental arrangement. The electromagnet is capable of magnetic flux densities up to 8 KGauss $\hat{=}$ 0.8 Vs/m^2. This arrangement allows the number of free carriers to be determined with an accuracy of 5 percent.

3.8 Resistivity Measurement. The resistivity measurement is useful in computing the value of n_r as seen in Equation 3.6.4 as well as giving a confirmation of the Hall effect measurement. Balancing the AC bridge gives the crystal resistance R_x.

3.9 Lifetime Measurement. In addition to the lifetime (τ) as determined from $S_i(f)$ in Equation 2.2.9, τ was measured with the apparatus as shown in Figure 3.9.1. The "Semiconductor Lifetime Measuring Equipment" emits a short duration (<1 µs) high intensity light pulse

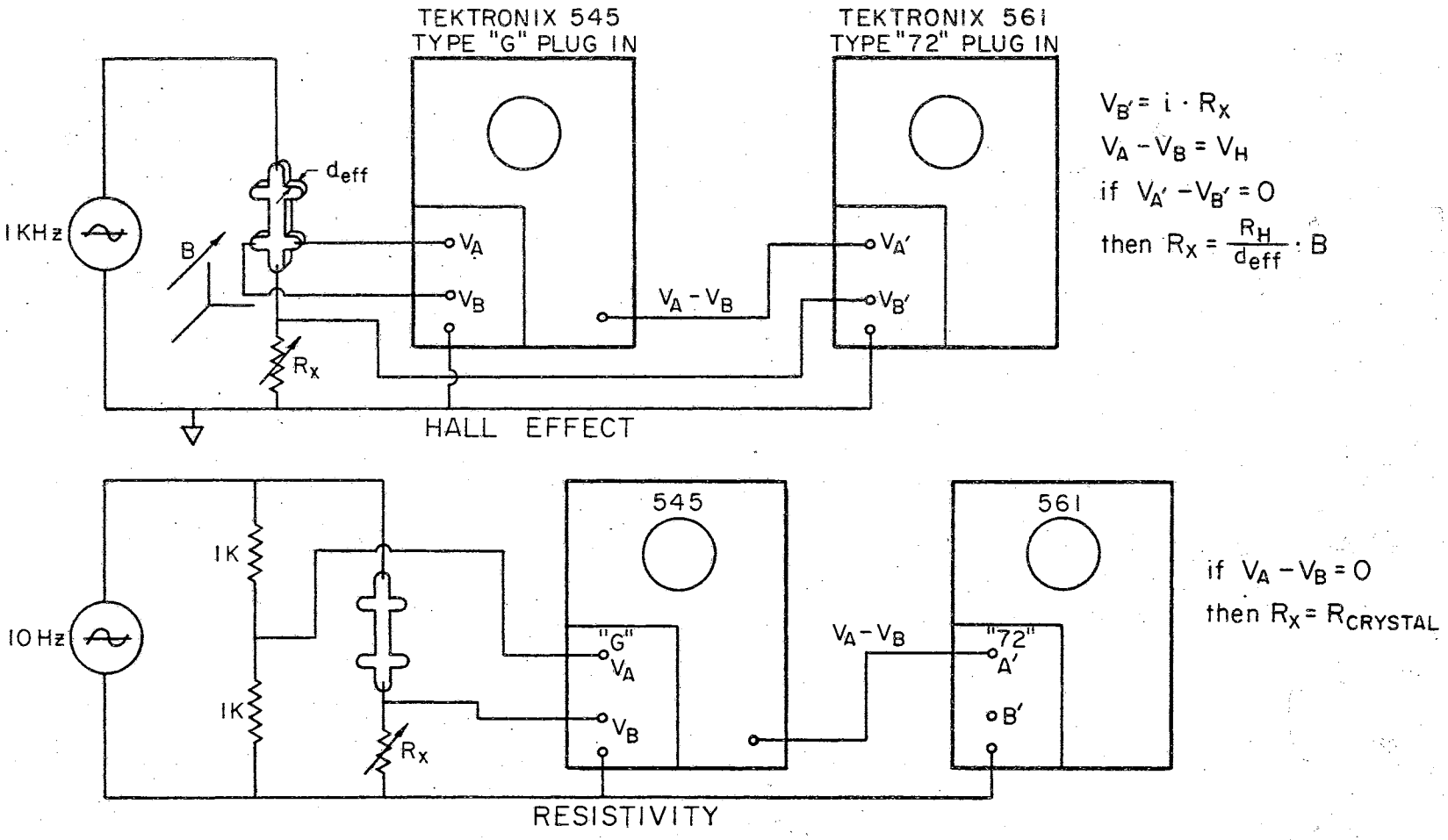

Figure 3.7.1. Experimental Arrangement for Hall Effect and Resistivity Measurements

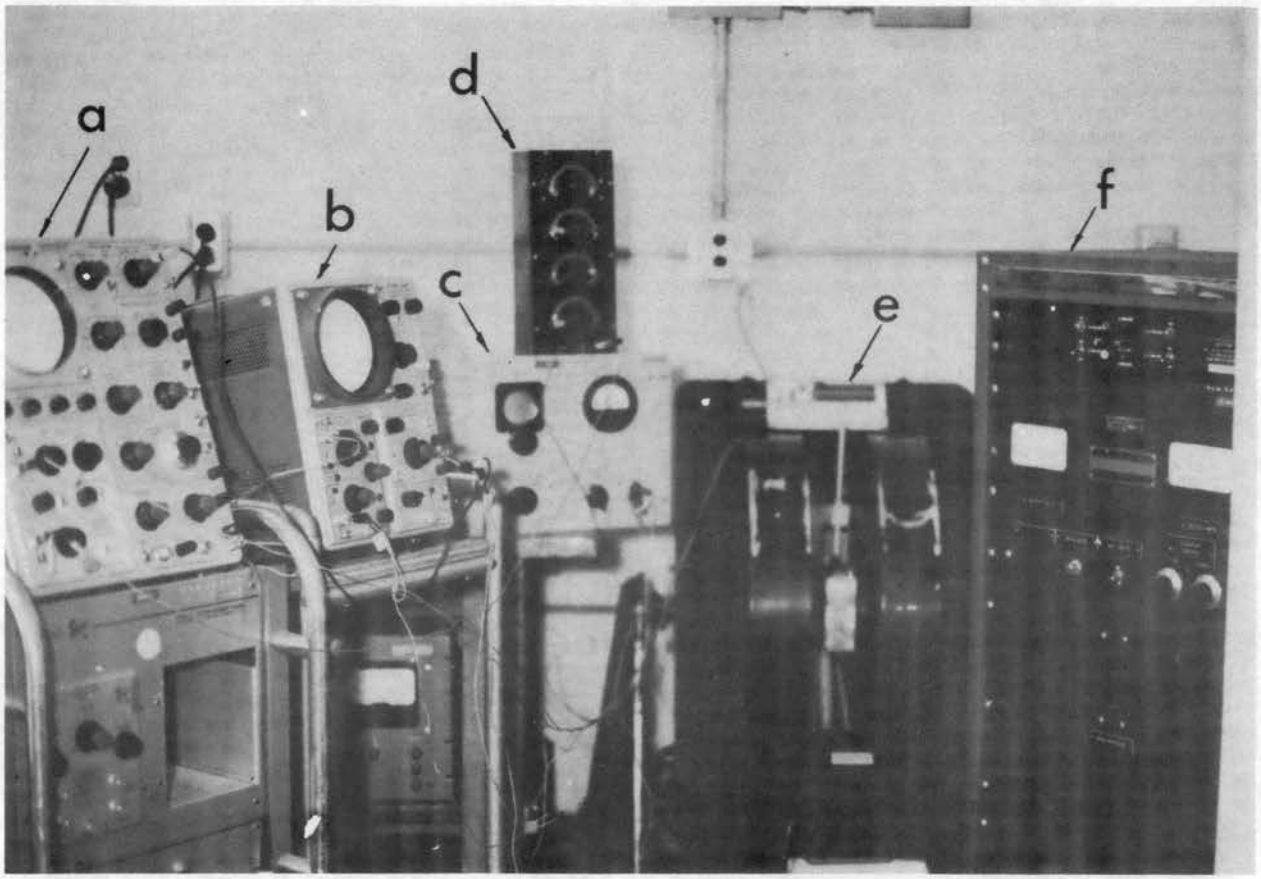

Figure 3.7.2. Hall Effect Measuring Setup

a. Tektronix 545
b. Tektronix 561
c. Oscillator
d. R_X
e. Magnet
f. Magnet Power Supply

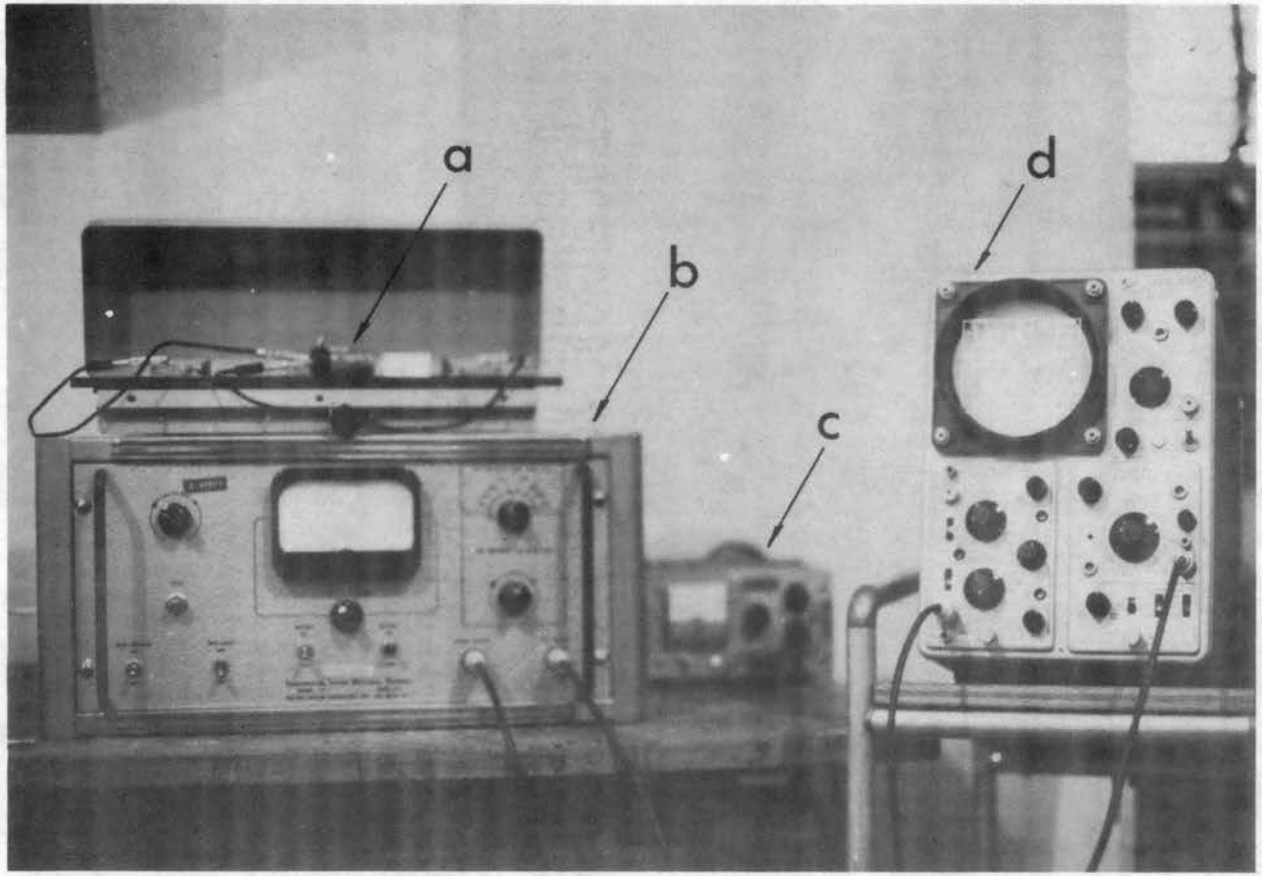

Figure 3.9.1. Photoconductive Lifetime Measuring Equipment
a. Crystal
b. Lifetime Meter
c. Power Supply
d. Oscilloscope

which is focused on the crystal. The decay of carriers induced by this light pulse is observed on the calibrated oscilloscope. A set of teflon filters was fabricated to allow variation of the light intensity in a controlled manner. The crystal current supplied by internal batteries or by an external well-regulated power supply can also be varied by a front panel control.

3.10 Crystal Preparation. A great deal of care is necessary in preparing a crystal with all of the necessary qualities for making a good noise measurement. The crystal piece is first cut into slices of the required thickness, and then an ultrasonic cutter is used to cut the sample shapes as shown in Figure 3.10.1 (the help of the Department of Electrical Engineering, University of Minnesota, is gratefully acknowledged for these two steps). The sample is then drilled in each contact area to provide a clearance hole for a 0.012 in. dia. stainless steel wire. A S. S. White industrial abrasive cutter is used for this operation. The air pressure is then reduced on the cutter from 100 psi to 60 psi, and the entire crystal is lightly sand blasted. Taking extreme care to keep the surface clean after the sand blasting, one-half of the sample is rhodium plated with an A-31 plating solution available from the Sigmund Cohn Corporation. A current of 4 mA for 30 minutes is used with a platinum anode during the plating. The sample is then washed in water, dried, and the unplated portion of the sample is sand blasted and plated. The sample is again washed and the contact areas painted with a polystyrene dope such as "Q-DOPE," manufactured by G-C Electronics Corporation. An additional sand blasting is now applied to remove all plating material not covered by the polystyrene. A

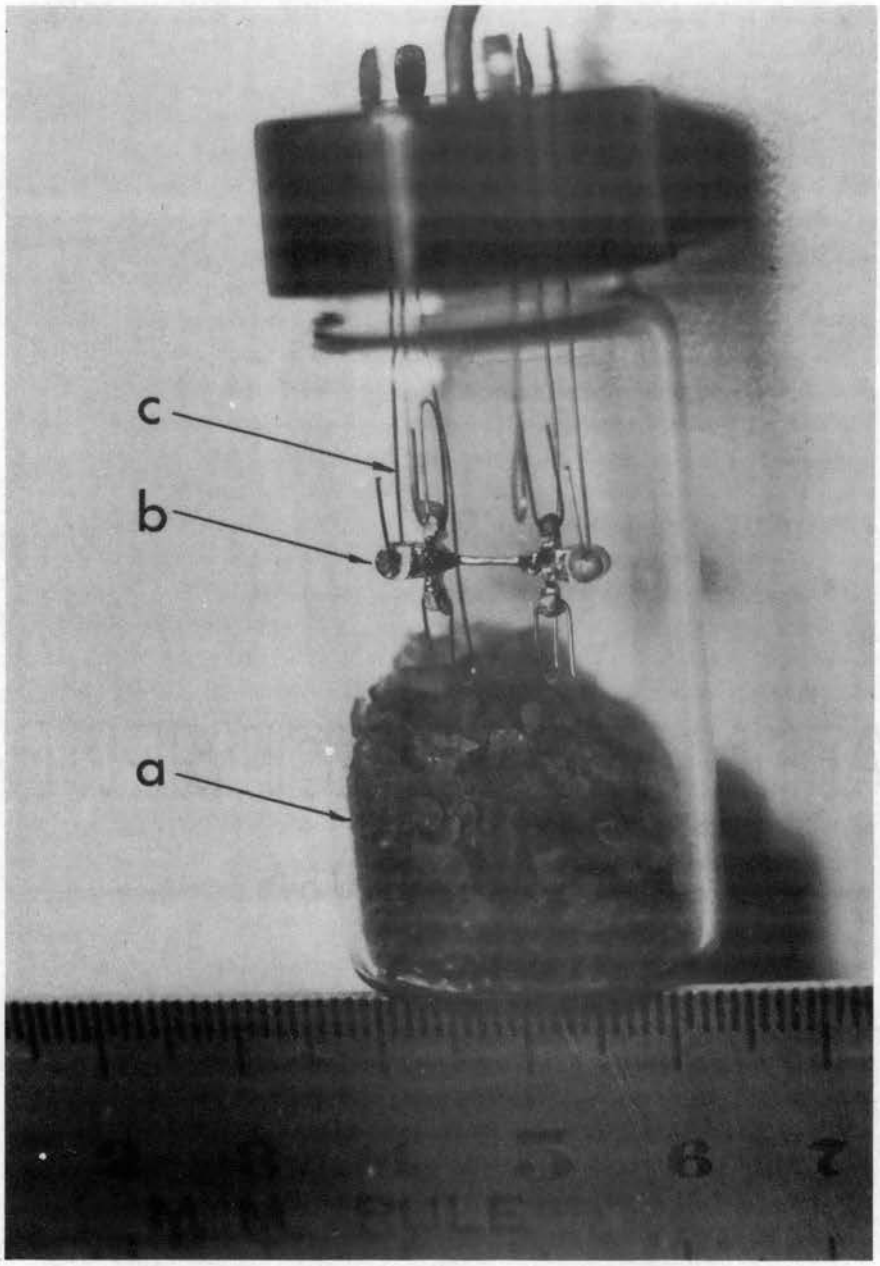

Figure 3.10.1 Short Bodied Ge-Single Crystal
a. Silica Gel
b. Crystal
c. Wires

polystyrene thinner is then applied to the sample which dissolves the polystyrene from the contact areas.

A sample holder is prepared using a glass vial, a brass plate with contact feedthroughs and a teflon gasket. Stainless steel wires (0.012 in. dia.) are attached to the crystal and feedthroughs as shown in Figure 3.10.1. The sample is then preheated to approximately 200°C and subsequently soldered using 60-40 tin lead high-quality solder and SAL-MET soldering flux (manufactured by Hascol Enterprises).

An etching solution of CP-10 is used to remove surface impurities and bring the crystal body down to the required size. The contact areas are coated with paraffin wax during this operation for protection against the etchant. When the sample body is reduced to the desired size, the wax is removed by heating, scraping, and then bathing the crystal in petroleum ether. The sample is then given an additional slight etch (5 seconds), washed in deionized water, rinsed in anhydrous methyl alcohol, and placed in the vial with a small quantity of silica gel crystals for drying purposes. The vial is then evacuated and filled with helium gas to a pressure of one atmosphere. A waiting time of approximately 48 hours is required before good noise measurements can be made due to the drying by the silica gel.

Samples with a much longer body are shown in Figure 3.10.2. These samples were formed using a pantograph in conjunction with the abrasive cutter. After the cutting, procedures as outlined above were followed in the final preparation of this type crystal.

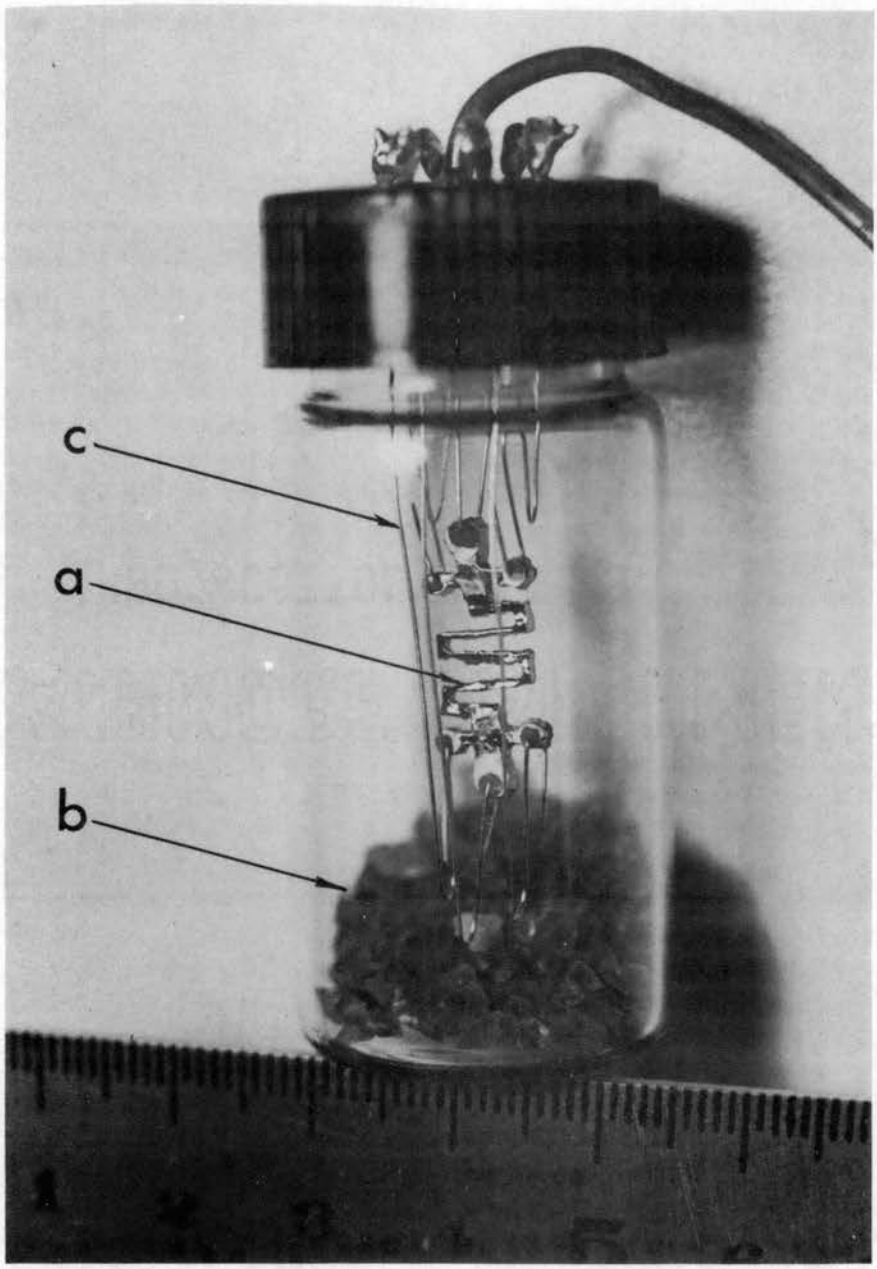

Figure 3.10.2. Long Bodied Ge-Single Crystal
a. Crystal
b. Silica Gel
c. Wires

CHAPTER IV

EXPERIMENTAL RESULTS OF IRRADIATED GERMANIUM SINGLE CRYSTALS

4.1 Introduction. The observed lifetime (τ) of a semiconductor containing two lifetimes τ_o and τ_1 is given by Kittel (16) as

$$\frac{1}{\tau} = \frac{1}{\tau_o} + \frac{1}{\tau_1} \qquad (4.1.1)$$

Letting τ_o be the initial lifetime and $\tau_1 = 1/\alpha\Phi$ (see Curtis-Cleland (9)) be the irradiation-induced lifetime, we have

$$\frac{1}{\tau} = \frac{1}{\tau_o} + \alpha\phi \qquad (4.1.2)$$

where

$\alpha_{neutrons} = 1.7 \times 10^{-8}$ (cm^2/neutron second) (9)

$\alpha_{^{60}Co\ gammas} = 1.67 \times 10^{-13}$ (cm^2/gamma second) (10)

ϕ = flux density (neutrons/cm^2, gammas/cm^2)

As an example, with an initial lifetime of 2 ms and 10^{12} 14.7 MeV neutrons/cm^2 irradiation, one would observe a lifetime of τ = 57 μs. If the same sample were irradiated with 10^{17} ^{60}Co gammas, then a τ = 58 μs would be observed.

For the particular effects that we wish to investigate in this thesis, a crystal is desired which has a low initial cutoff frequency (which corresponds to a large lifetime). This is desired because

τ = 1 μs is a reasonable lower limit of lifetime which can be achieved with fast neutron irradiation and with conventional gamma sources of 10^4 to 10^5 curies. Also, much less radiation damage need be introduced to achieve a given decrease in the initial lifetime. It is the purpose of this chapter to discuss some of the problems associated with obtaining a low initial cutoff frequency, how they were overcome, and the experimental results of a large (>10^3) change in the resulting cutoff frequency of fast neutron irradiated crystals. Some very interesting results will also be discussed regarding spectra obtained with gamma-irradiated crystals which cannot be explained by either multilevel recombination or ambipolar transport phenomenon.

4.2 Ambipolar Drift in Near Intrinsic Crystals. The first crystal samples which were prepared for measurement were of the type shown in Figure 3.10.1. Even though these samples were cut from a crystal whose bulk lifetime was 400 μs, the lifetime as measured first with the lifetime equipment (Figure 3.9.1) and second from the noise spectra, always fell short of this value by at least a factor of 3. This inconsistency was believed to be caused by the ambipolar (14) drift of the minority carriers (which we wish to avoid in this investigation), and the hypothesis was subsequently proven by three independent experiments.

The ambipolar drift time is given by

$$\tau_a = \frac{L}{\mu_a E} \qquad (4.2.1)$$

where

L = path length (m)

μ_a = ambipolar mobility (m^2/s)

E = field strength (volt/m)

As shown by Hill and van Vliet (14), τ_a is infinite in either a strongly n-type or intrinsic semiconductor but reduces to

$$\tau_a = \frac{L}{\mu_p E} \qquad (4.2.2)$$

in a near intrinsic n-type semiconductor which is our particular case for the region of interest in g-r noise measurements. The reasoning is as follows: Fluctuations in a near intrinsic semiconductor are generated as electron-hole pairs. If a fluctuation is generated at a particular spot in the semiconductor, the increase in conductivity causes electrons to move everywhere in the crystal simultaneously towards the positive end of the crystal. Therefore, electrons flowing out of the region of increased conductivity will not cause an increase in the adjacent region because electrons are leaving the adjacent region at the same rate. However, the holes flowing toward the negative terminal are mainly neutralized by electrons flowing in the opposite direction. The carriers arrange themselves continually so that $\Delta n = \Delta p$. The region of increased conductivity, therefore, moves toward the negative terminal with approximately the hole mobility and decays in amplitude with the minority carrier lifetime.

The ambipolar effect was confirmed by directing the light pulse in the lifetime meter on opposite ends of the long crystals as shown in Figure 3.10.2. τ readings of 130 and 580 μs were obtained as the light was directed near the negative and positive ends of the crystal, respectively.

A further confirmation was made by measuring $S_i(f)$ as a function of I for the small crystal as shown in Figure 3.10.1. Since I is

proportional to E, we can confirm the dependence of τ_a through Equation 4.2.1 and the noise spectrum. The results are given in Table I.

TABLE I

CURRENT DEPENDENCE OF CUTOFF FREQUENCY AND NOISE RATIO OF CRYSTAL NO. 2

I	f_c	n_r
mA	KHz	Relative
0.11	2.5	1
0.315	4.7	3.8
1.0	15	12

It can be readily seen that the decrease in τ_a ($= 1/2\pi f_c$) compensates the increase in I so that n_r is proportional to I.

The third confirmation was obtained with the g-r spectrum of a long crystal as in Figure 3.10.2. After preparing the surface and contacts the same way as the shorter crystal, a much lower cutoff frequency ($= 1/2\pi\tau$) was immediately obtained. The spectra obtained with this type crystal will be discussed in the next section.

4.3 Results of Fast-Neutron Irradiation Experiments. The experiments with fast-neutron irradiation were conducted on the long type crystals. Two crystals of this type were prepared for the purpose of serving as a check against each other. The results of crystal no. 9, which received the largest neutron dose, will be discussed first.

Crystal no. 9 was irradiated in four steps. Although no precise

measurements of the neutron flux could be made at the time of irradiation due to inability in determining the exact distance from the source to the sample, a good indication is obtained from correlation with lifetime vs. neutron dose data (2, 9) and from Cleland-Bass (7) who report 12 electron removals (cm^{-1}) per incident 14.1 MeV neutron. 14.7 MeV neutrons were used in this thesis. Our experiments show that 2.4×10^{14} electrons have been removed which indicates an effective total dose of 2×10^{13} n/cm^2. From the Curtis-Cleland (9) data, this corresponds to a τ of 3 μs, which moderately agrees with our measured value of 2 ± 0.5 from the $S_i(f)$ data (the given uncertainty arises mainly from measurements at different temperatures).

Before and after each irradiation step, the g-r spectra, Hall effect, and resistivity were measured. The results of the g-r spectra were used to plot τ as shown in Figure 4.3.1. These data are presented in this form which allows the results of the cutoff frequencies of all the g-r spectra to be viewed on one compact figure while avoiding the confusion of many overlapping g-r curves.

The lifetime data from Figure 4.3.1 was obtained from the g-r spectra by picking the points on the curves corresponding to $S_i(f_c)/S_i(f \to 0) = 1/2$. In the majority of the cases, the curves were of the form $1/(1 + \omega^2 \tau^2)$ with one exception being at some temperatures before irradiation. At the temperature of 39°C ($1/T = 3.04 \times 10^{-3}$ $^\circ K^{-1}$), the data fit the theoretical form very well before irradiation; however, at the other temperatures, the data in the region $\omega > 1/\tau$ went as $1/\omega^n$ where $n < 2$. Another exception occurred after the third irradiation. Here the crystal has been converted to slightly p-type with an effective doping of 1.6×10^{12} acceptors. The spectra for 23.5°C ($1/T =$

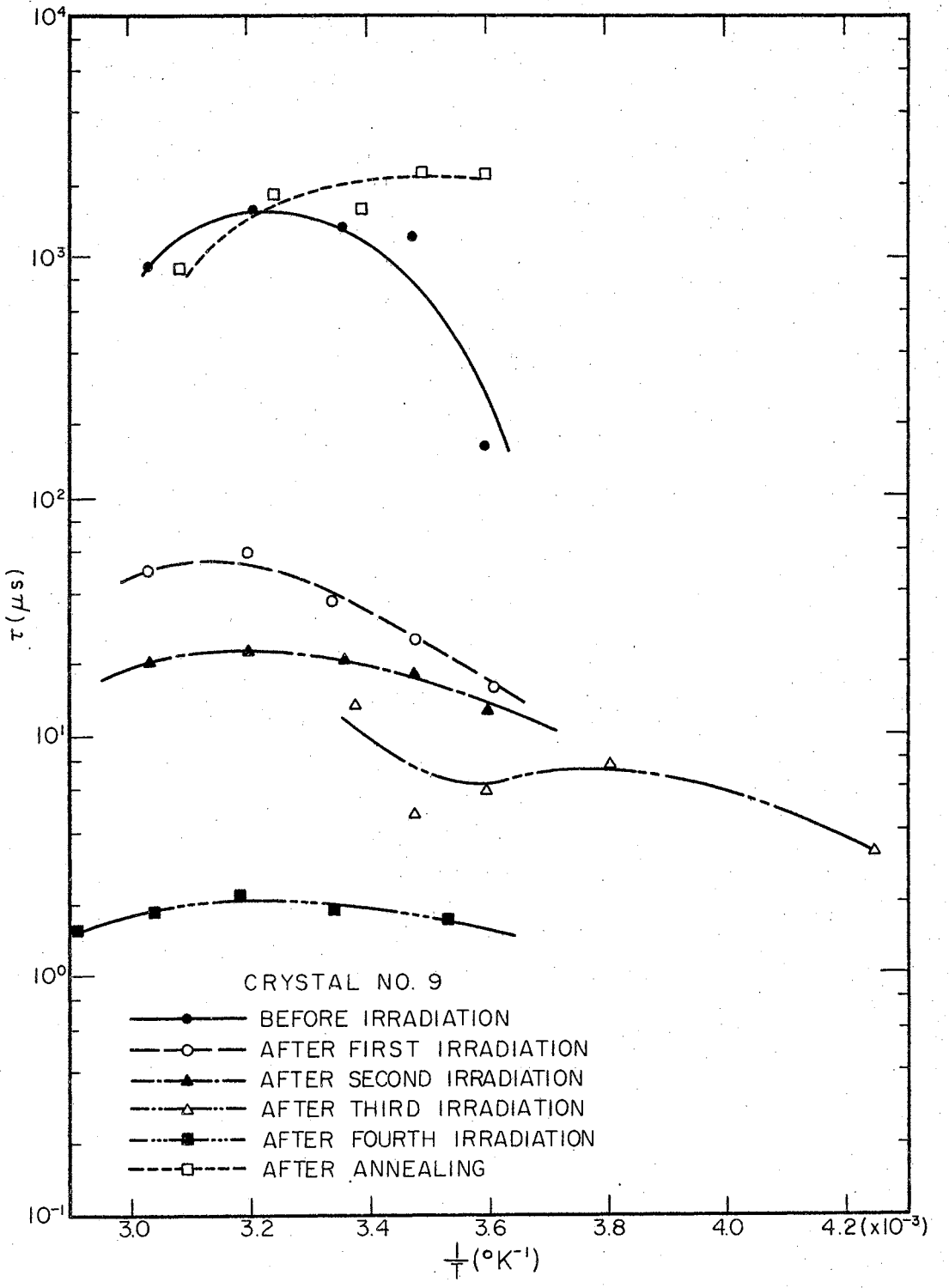

Figure 4.3.1. Lifetime Vs. 1/T for Crystal No. 9 Before Irradiation, After Various Degrees of Neutron Irradiation, and After Annealing for 70 Minutes at 550°C

3.38×10^{-3} $^{\circ}K^{-1}$) followed $1/\omega^2$ at the higher frequencies, but for lower temperatures the slope became increasingly less until at -11°C ($1/T = 3.81 \times 10^{-3}$ $^{\circ}K^{-1}$) the curve contained a slope of 1/2 beyond the corner frequency. Also, more scatter is observed in the τ measurements after the third irradiation than in the other cases. The τ vs. 1/T curves agree with the Shockley-Read (25) theory of having a maximum when the Fermi-level is in the center of the energy gap. A lifetime change from an initial value of 2 ms to a final value of 2 μs after 2.7×10^{13} neutrons/cm^2 has been accomplished.

4.4 Results of Annealing. The crystal was then annealed at 550°C for 70 minutes. The glass vial and teflon gasket were removed, and the crystal assembly placed inside a ceramic cylinder which shielded the crystal from the heating element. The heat was accomplished by three turns of 0.040 in. tungsten wire around the ceramic cylinder. Approximately 25 amperes through the wire was required to reach 550°C. An external copper shield was provided for the entire assembly which acted as an infrared reflector and allowed a lower operating temperature to be used on the tungsten heating element. The entire system was in a 10μ Hg vacuum during the annealing process. After annealing, the crystal was given a slight etch to restore the surface lifetime, subsequently placed in the vial, and allowed to dry 24 hours before measurements were resumed.

4.5 Discussion of Fast-Neutron Irradiation and Annealing Results. Figures 4.5.1 and 4.5.2 show the n_r curves. The theoretical shape of these curves is illustrated in a paper by Bilger and McCarter (2) and the location of the peak given as:

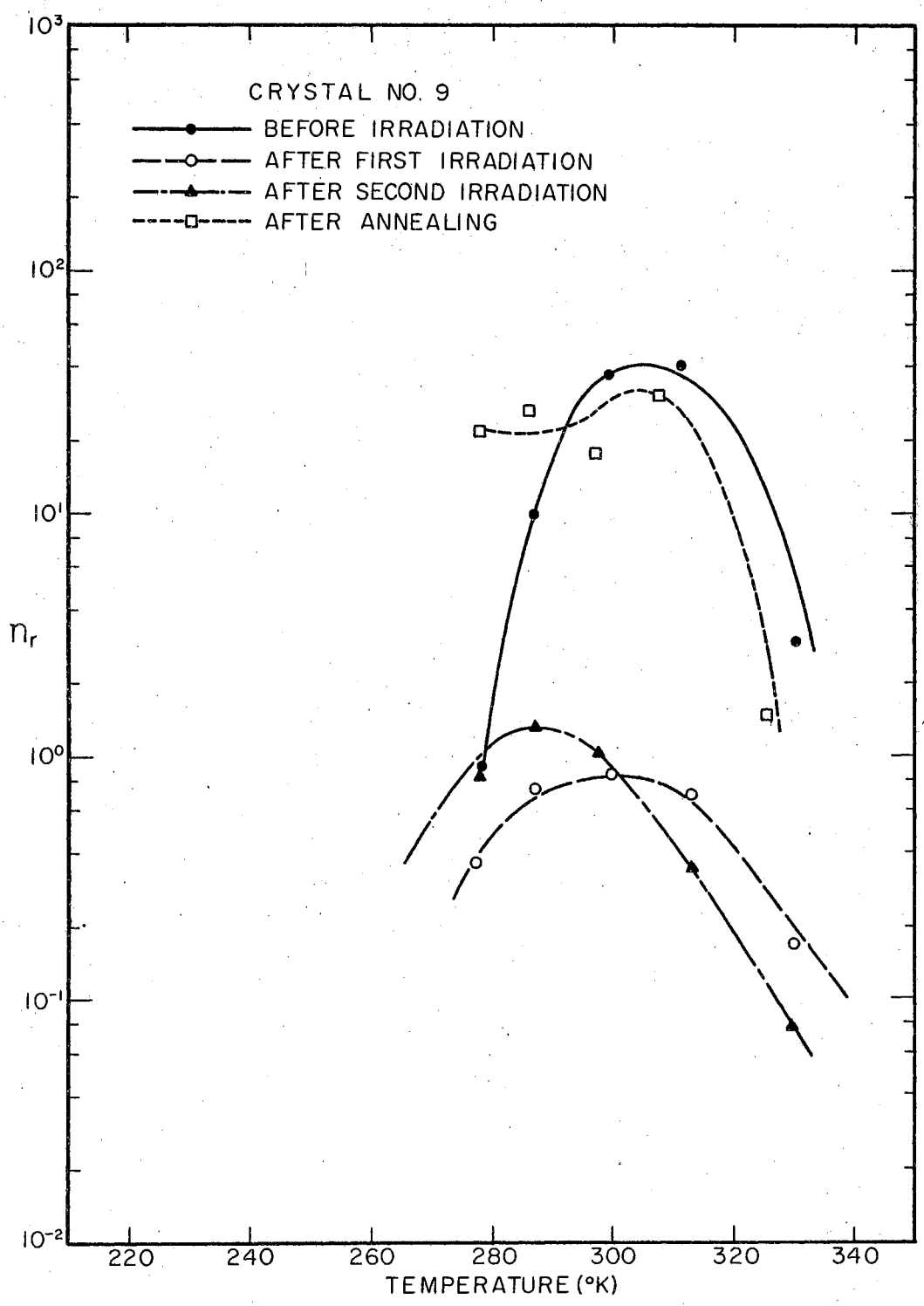

Figure 4.5.1. Measured n_r Vs. T Curves for Crystal No. 9. All Curves are Normalized for 0.1 mA Crystal Current

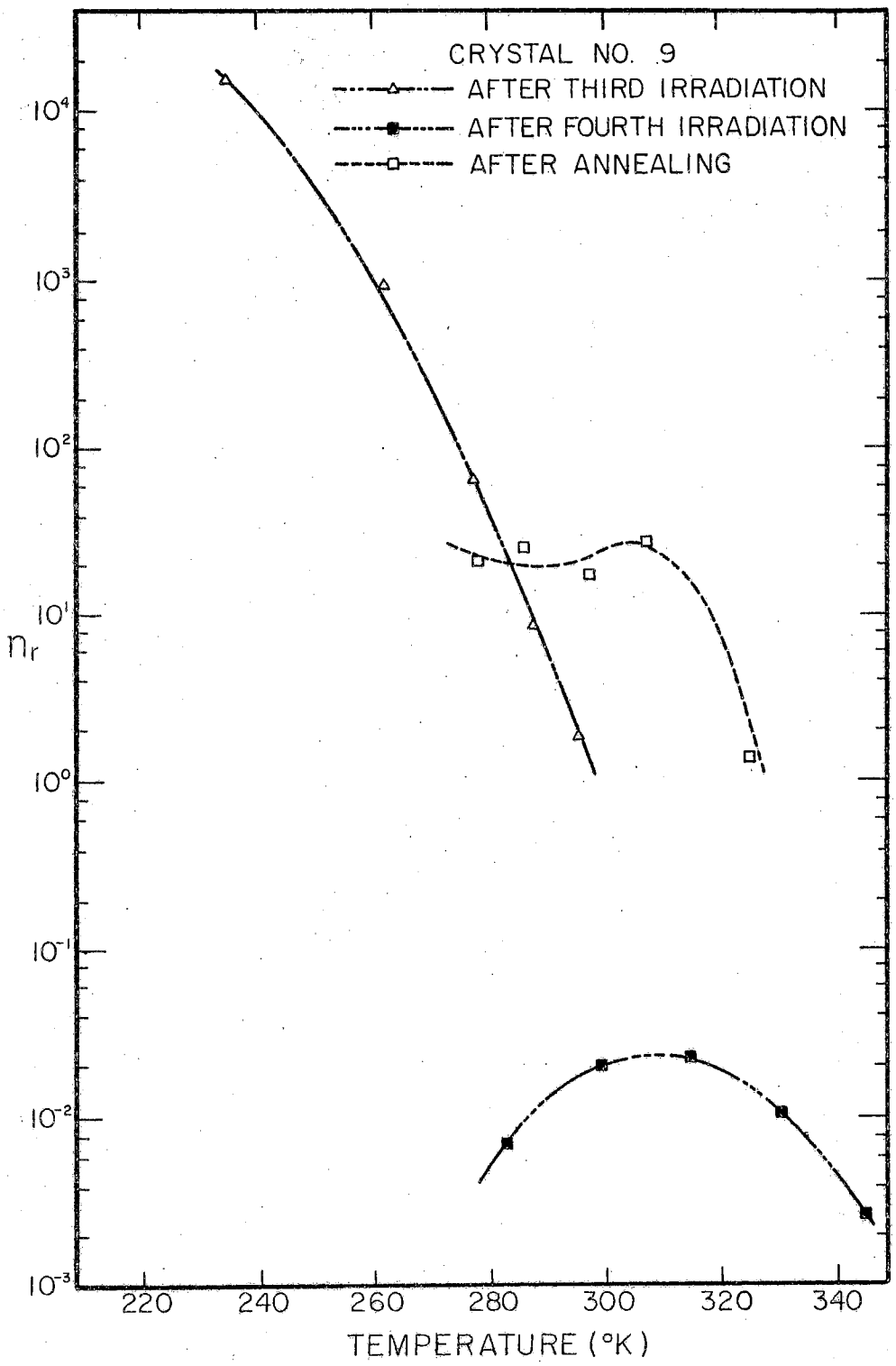

Figure 4.5.2. Measured n_r Vs. T Curves for Crystal No. 9. All Curves are Normalized for 0.1 mA Crystal Current

n material: $(p/n)_{peak} \approx 0.21$ or $n_i \approx 3/5\ N_D$

p material: $(p/n)_{peak} \approx 8.2$ or $n_i \approx 2/5\ N_A$

These curves give a good match to the theoretical curves except after annealing where n_r remains high at temperatures below the peak value. This deviation was also reported by Bilger and McCarter (2) after annealing of neutron irradiated gold doped Ge-crystals. A very large n_r range of 10^7 can be seen from Figure 4.5.2. This range was probably even larger than the measurements indicate as the peak was never reached after the third irradiation due to temperature limitations of the measuring equipment.

Hall effect results are shown on Figures 4.5.3 and 4.5.4. The crystal converted from n to p type after the third irradiation. The reversal in R_H provides a point independent of crystal dimensions for determining the amount of each kind of free carriers as can be seen from Equation 3.7.2. This method (using b = 2.11) was used to calculate the effective doping for the p-type crystals in Table II. For the n-type crystals, R_H is proportional to 1/n in the extrinsic range; so, knowing the initial value of 4×10^{13} antimony atoms/cm^3, one can readily estimate the effective doping using the Hall effect data. In some cases the curve is not flat in the extrinsic range, so the estimate could have a much greater error than cases where a flat portion is obtained. Equation 3.7.2 was always used to calculate doping changes, even though it is very possible that the mode of scattering may change with irradiation and cause a change in the coefficient of R_H. The manufactures doping (4×10^{13} N_D/cm^3) was used for normalization. After annealing, the effective doping returned to within 20 percent of the

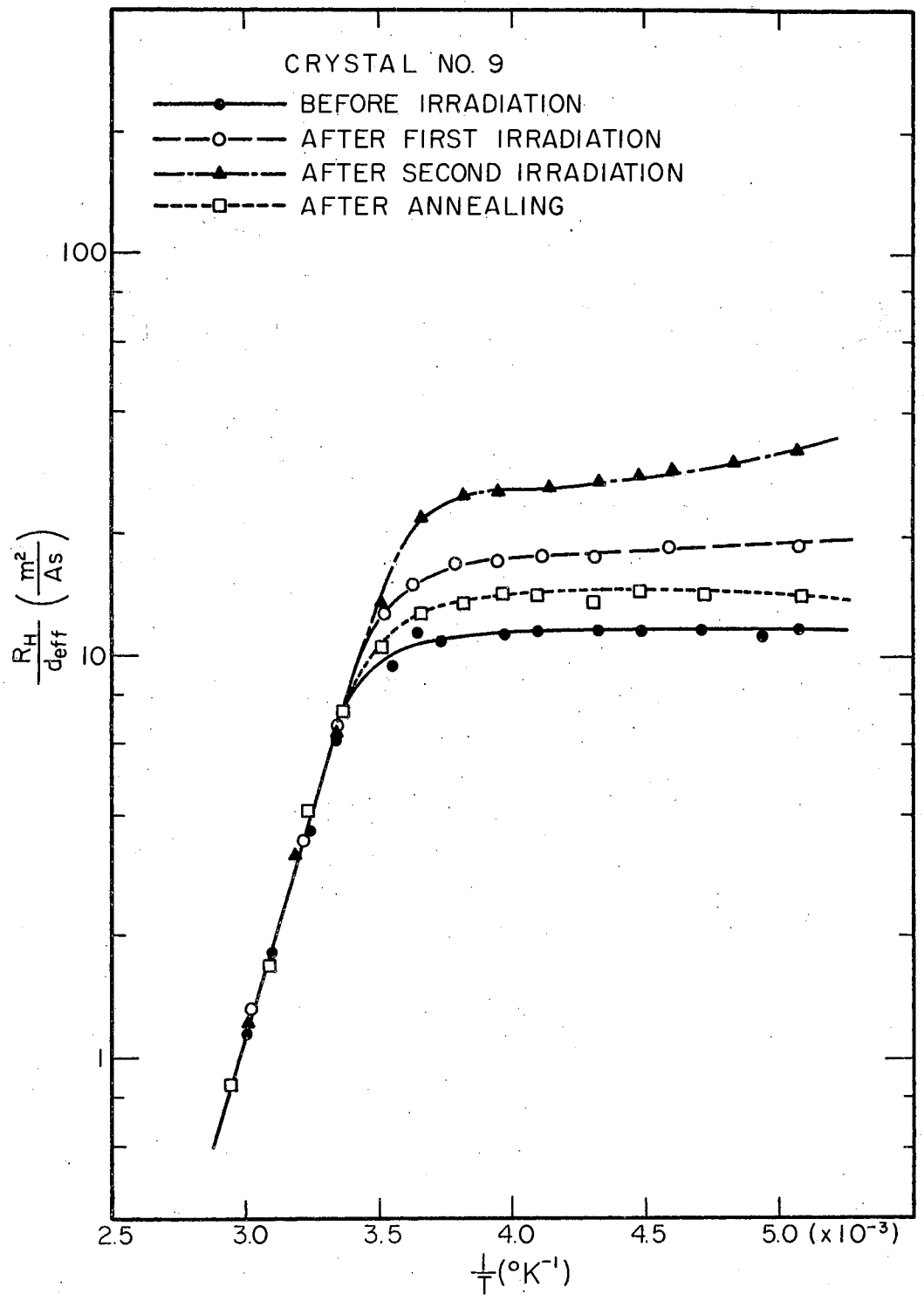

Figure 4.5.3. Hall Effect Vs. 1/T for Crystal No. 9 Before Irradiation, After First and Second Irradiation, and After Annealing

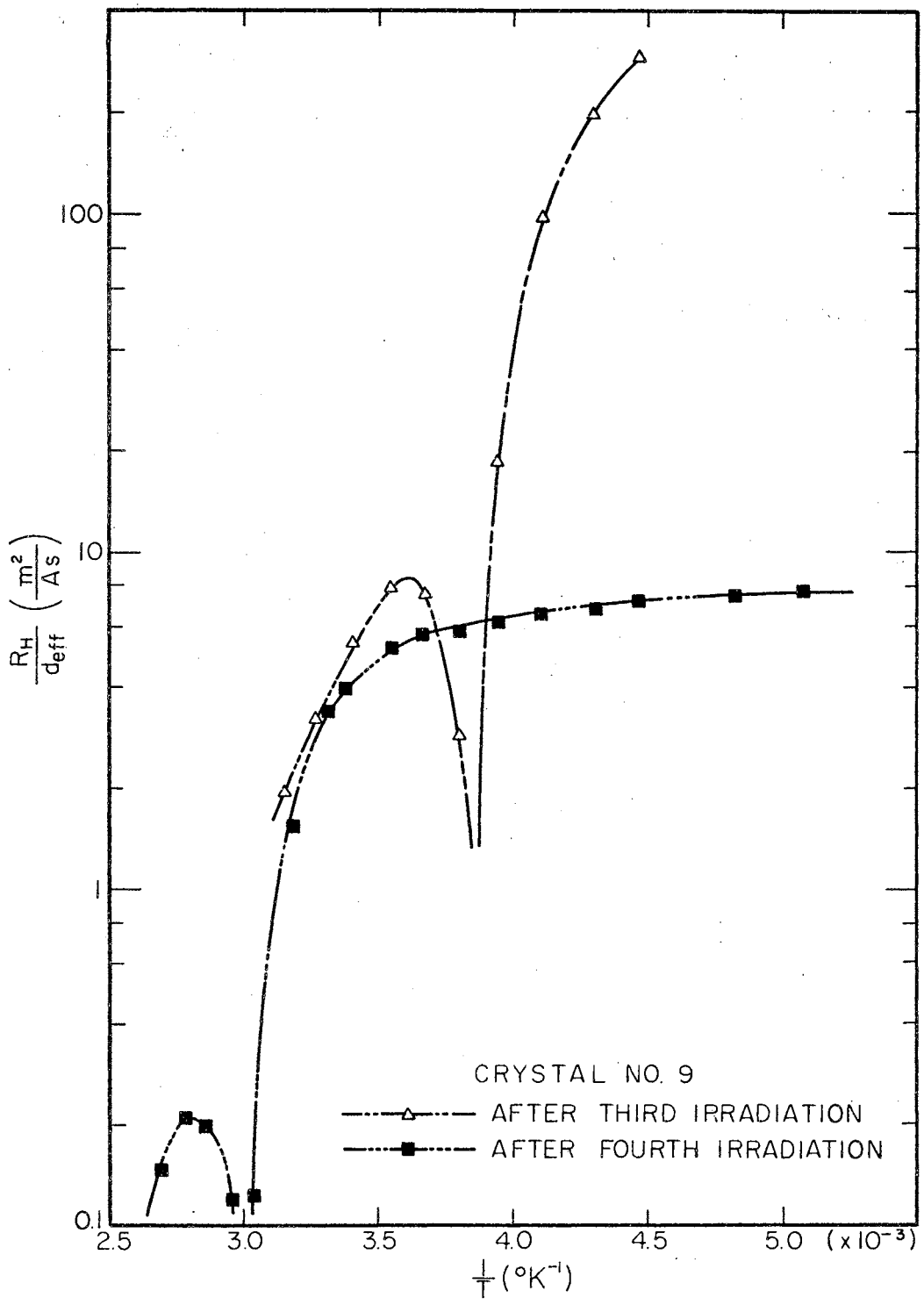

Figure 4.5.4. Hall Effect Vs. 1/T for Crystal No. 9 After Third and Fourth Irradiation. Crystal is now p Type

initial n-type value.

Resistivity data are shown in Figures 4.5.5 and 4.5.6. These data give a confirmation of the Hall effect in determining the number of carriers. The resistance data are also used in the determination of n_r.

Table II gives a compilation of the lifetime data (τ) as determined by the photoconductive lifetime meter, the cutoff frequency (f_c) from the g-r noise spectra, the n_r values, and the effective doping. Values from measurements near room temperature were used for the data in this table.

TABLE II

SUMMARY OF RESULTS FROM CRYSTAL NO. 9

	τ(μs)	f_c (KHz)	n_r (I_{DC} = 0.1 mA)	Effective Doping
Before Irrad.	580	0.12	38	n-type 4×10^{13}
After 1-st Irrad.	56	4.4	0.9	n-type 2.7×10^{13}
After 2-nd Irrad.	36	7.8	1.0	n-type 1.7×10^{13}
After 3-rd Irrad.	24	12	1.0	p-type 1.6×10^{12}
After 4-th Irrad.	5	85	0.02	p-type 2×10^{14}
After Annealing	320	0.1	18	n-type 3.2×10^{13}

Representative g-r spectra for near-room temperatures and I_{DC} of 0.1 mA are shown in Figure 4.5.7. The increase in cutoff frequency by a factor of 10^3 and a corresponding decrease in $S_i(f)$ is readily apparent as the irradiation is increased. Annealing returns the spectra

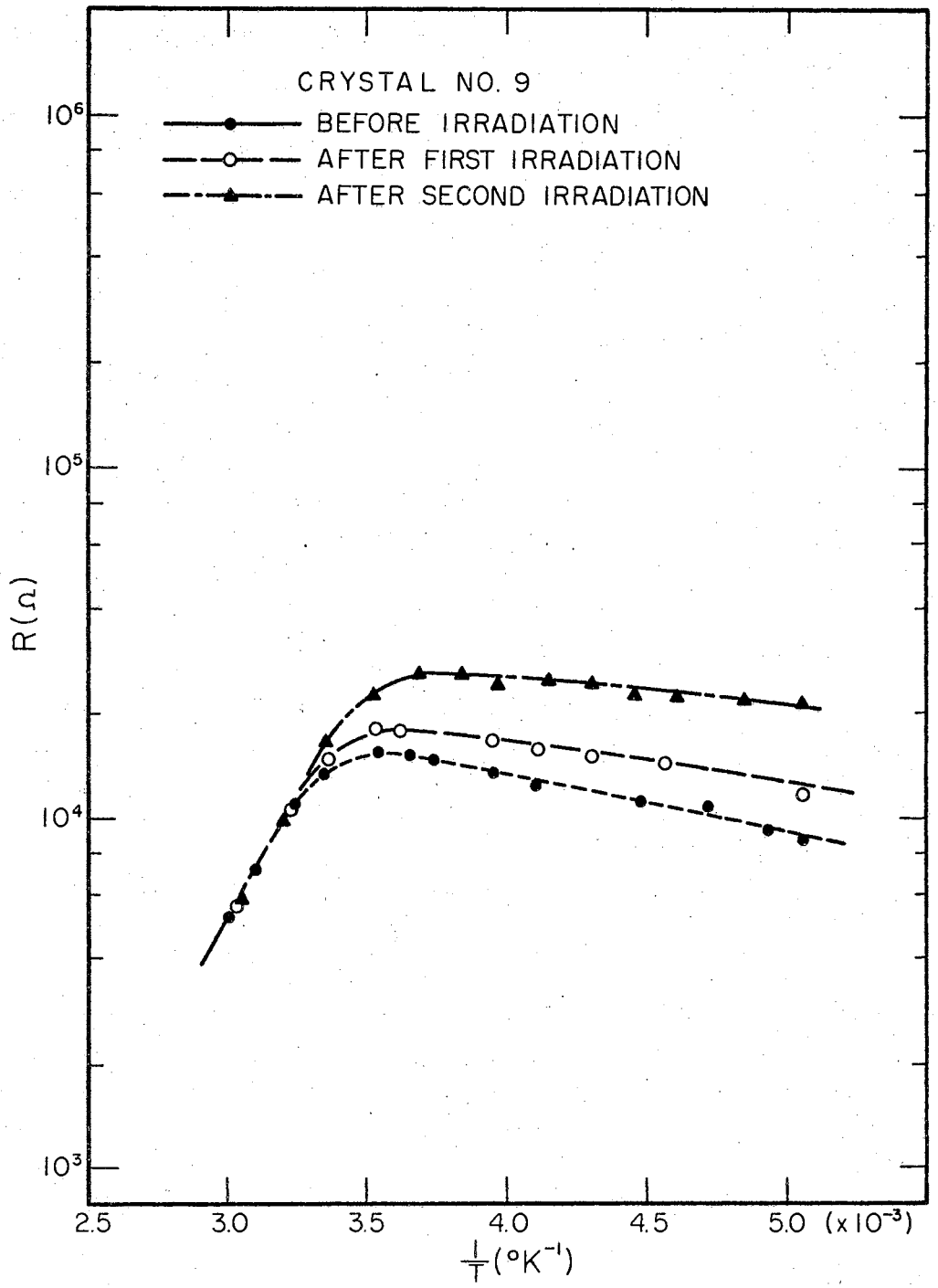

Figure 4.5.5. Resistance Vs. 1/T for Crystal No. 9 Before and After the First Two Irradiations

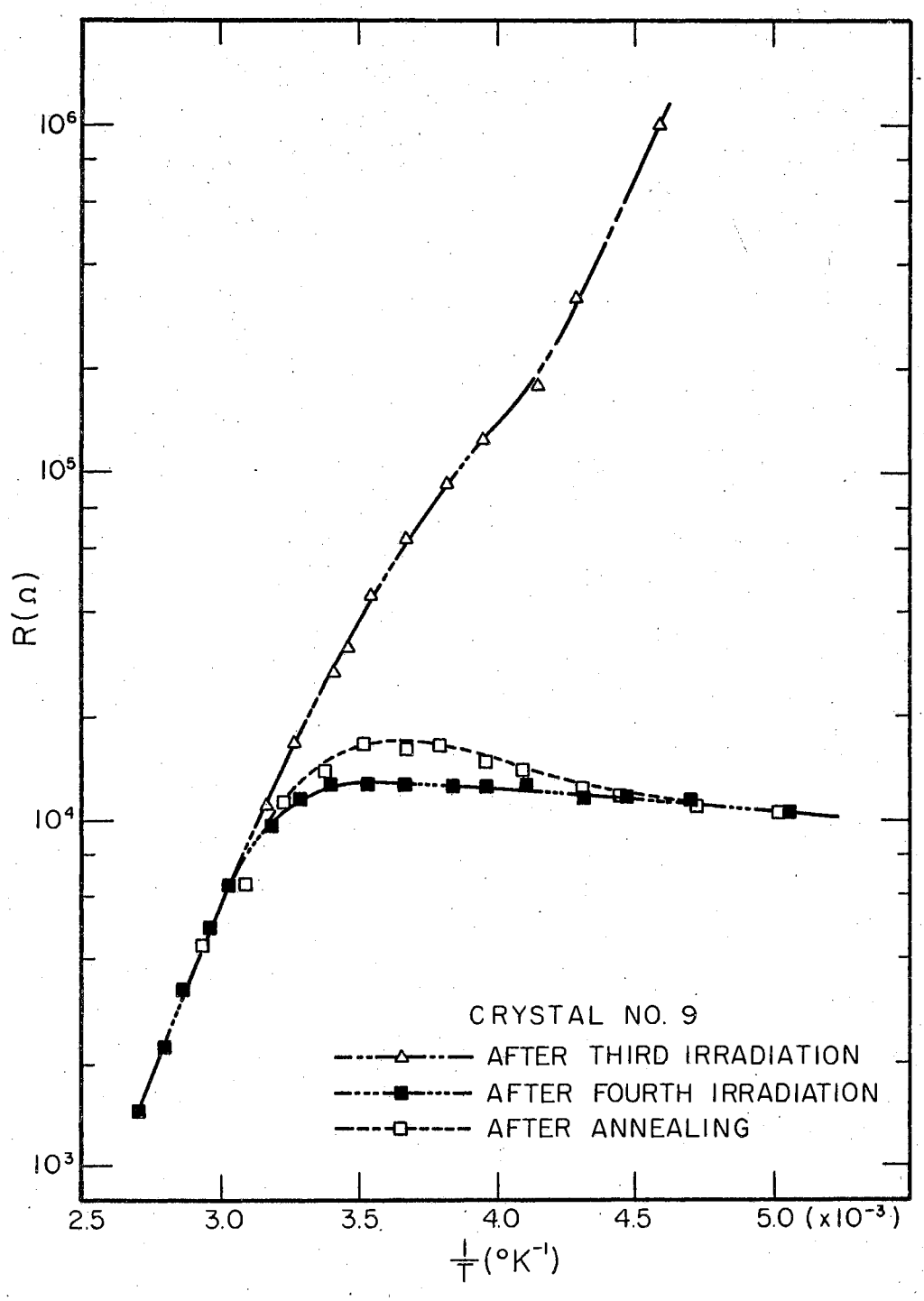

Figure 4.5.6. Resistance Vs. 1/T for Crystal No. 9 After Third and Fourth Irradiation and After Annealing

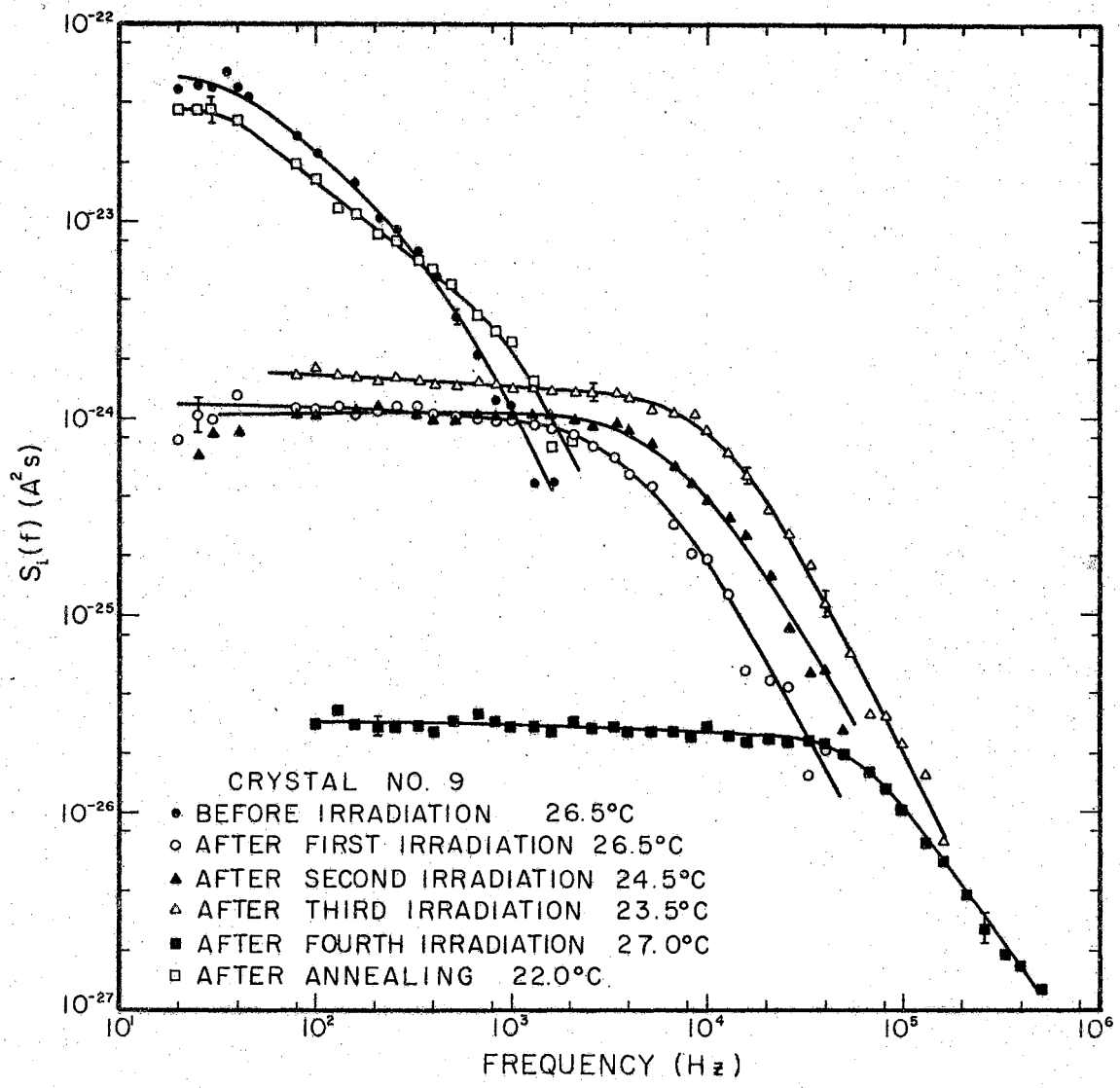

Figure 4.5.7. Representative G-R Spectra for Crystal No. 9 Near Room Temperature. All Curves are Normalized to 0.1 mA Crystal Current

very near to the initial value. The slope is not 2 in the region above cutoff for the initial spectra; but, after each irradiation, we have slopes of 2 in the corresponding regions despite the fact that we know we create complicated lattice defects with irradiation (10). After annealing, we obtain almost an identical spectrum to the initial, which indicates that the initial defects are of a consistent nature.

Sample no. 10 was cut from the same crystal as no. 9 and was also used in the neutron irradiation experiments as confirmation of the results from no. 9. Figure 4.5.8 shows that the lifetime agrees well with the results from sample no. 9 before irradiation and after annealing. The total neutron dose for no. 10 was much less than for no. 9, so the lifetime was only reduced to 20 μs (a factor of 10^2 from the initial point) at room temperature.

One of the differences in the two crystals can be noted on Figure 4.5.9 where n_r (peak) was a factor of 20 larger than the n_r (peak) from no. 9 before irradiation. Correspondingly, the slope of the g-r spectra for no. 10 was 2.2 as compared with 1.8 for no. 9 and $f_c(9)/f_c(10)$ was 1.37. However, after annealing (500°C, 30 minutes), the lifetimes and slopes of no. 10 compared favorably with those of no. 9 before irradiation, which indicates that the neutrons produce some defects which do not anneal. One additional difference occurred in that the n_r of no. 10 after annealing returned again to the theoretical shape. This is attributed to the lighter neutron dose.

The Hall effect and resistance data for crystal no. 10 are shown in Figures 4.5.10 and 4.5.11. Using this data, we obtain an electron removal of 2.7×10^{13} cm^{-3} which corresponds to a neutron dose of 2.25×10^{12} n/cm^2 and a lifetime of 25 μs. This agrees well with the lifetime

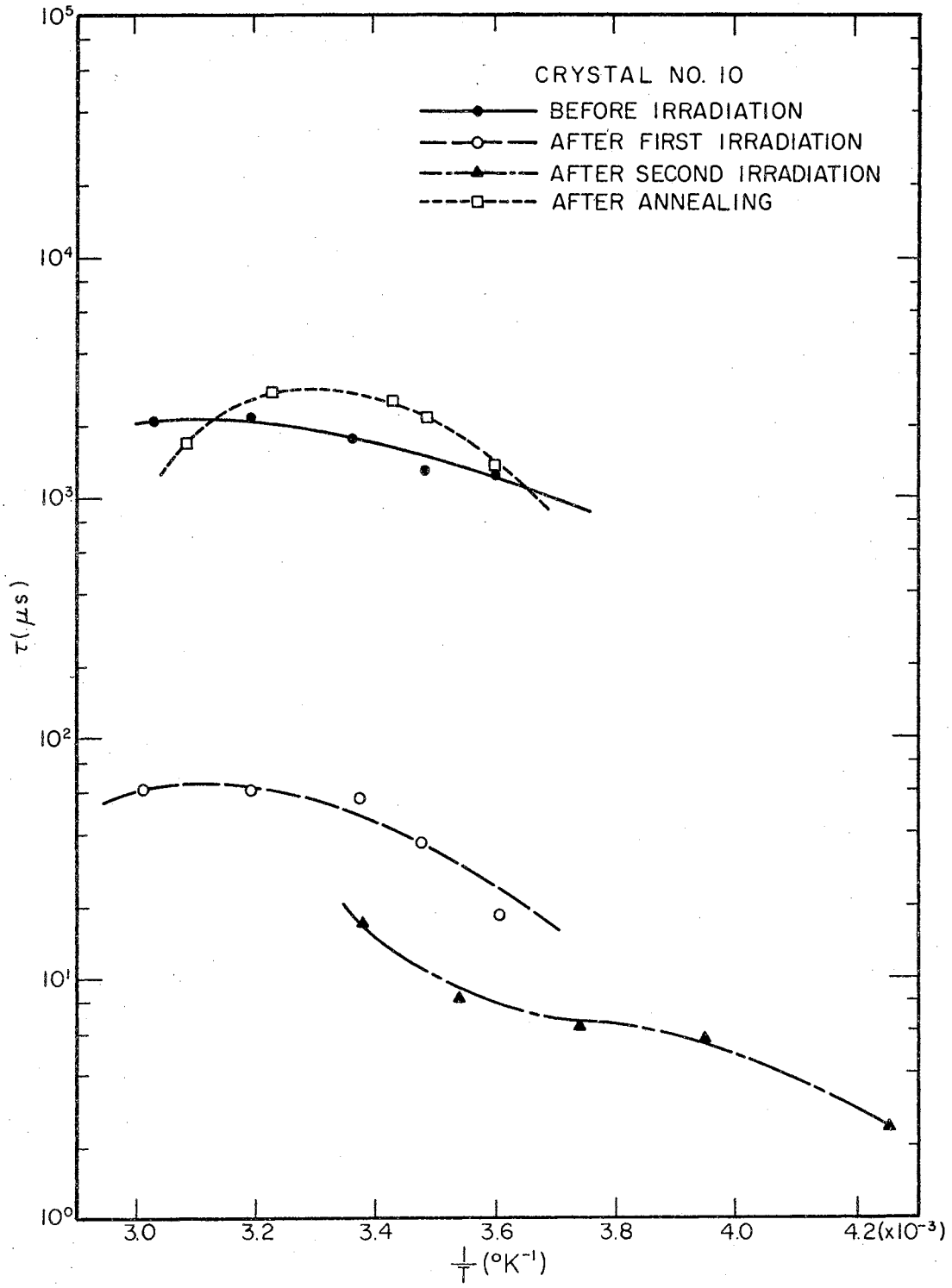

Figure 4.5.8. Lifetime Vs. 1/T for Crystal No. 10 Before Irradiation, After First and Second Irradiation, and After Annealing

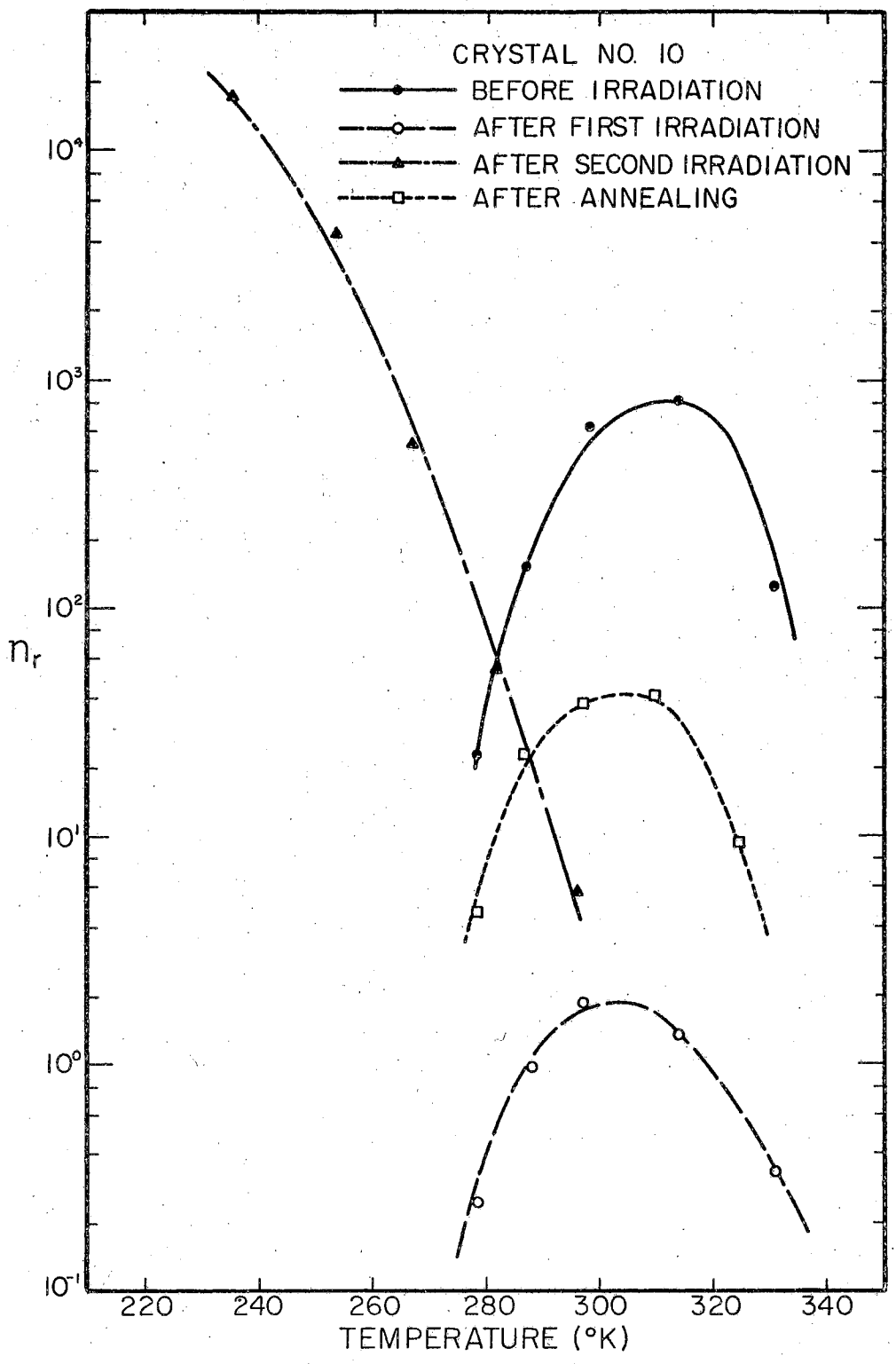

Figure 4.5.9. n_r Vs. T for Crystal No. 10. All Curves are Normalized to 0.1 mA Crystal Current

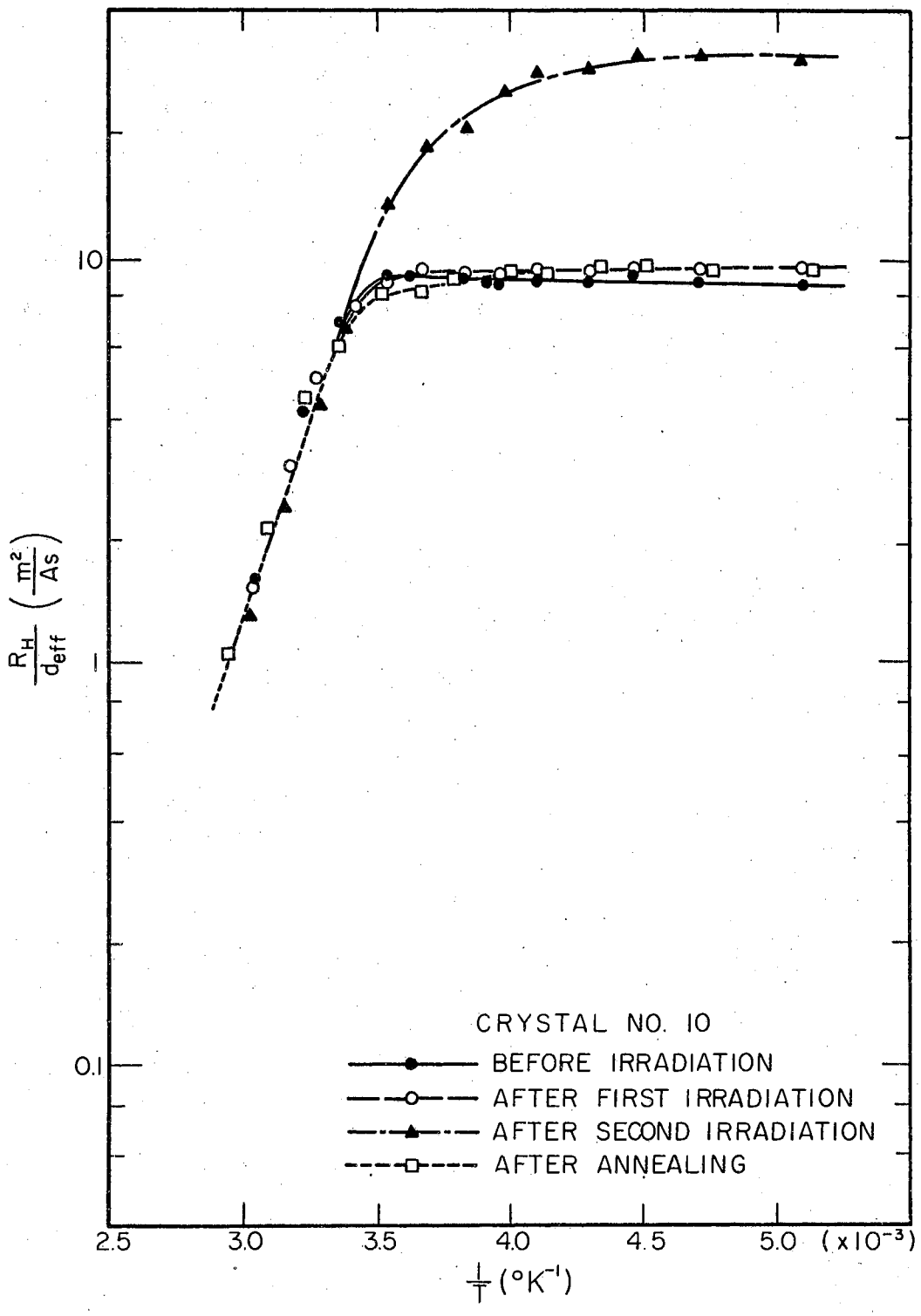

Figure 4.5.10. Hall Effect Vs. 1/T for Crystal No. 10. Compare With Figures 4.5.3 and 4.5.4

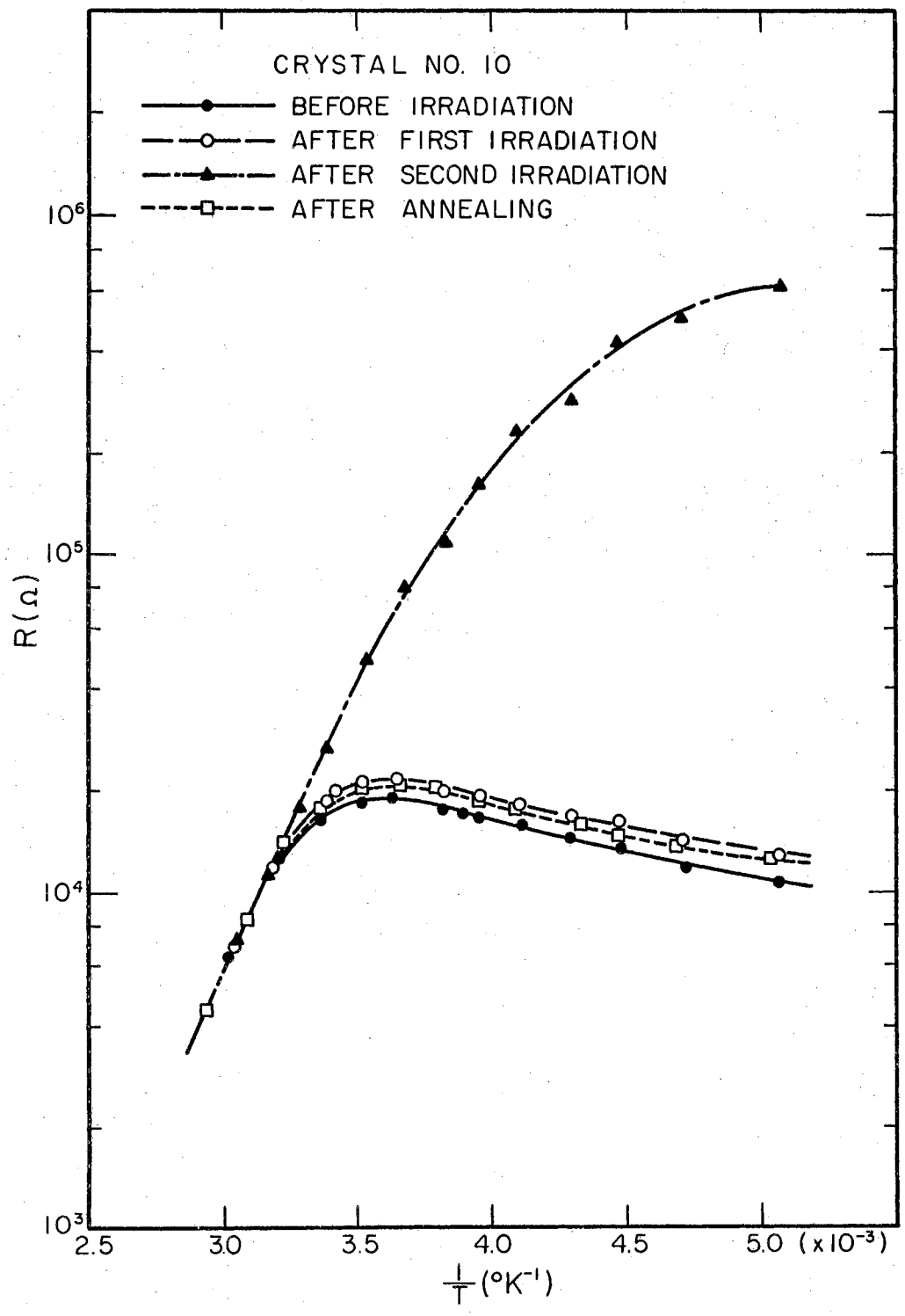

Figure 4.5.11. Resistance Vs. 1/T for Crystal No. 10. Compare With Figures 4.5.5 and 4.5.6

of 20 μs calculated from the g-r data at room temperature. Representative data are listed in Table III.

TABLE III

SUMMARY OF RESULTS FROM CRYSTAL NO. 10

	τ(μs)	f_c (KHz)	($I_{DC} \approx 0.1$ mA)	n_r Effective Doping
Before Irrad.	580	0.088	700	n-type 4×10^{13}
After 1-st Irrad.	100	2.75	2	n-type 3.8×10^{13}
After 2-nd Irrad.	23	11	6	n-type 1.3×10^{13}
After Annealing	320	0.064	40	n-type 3.9×10^{13}

4.6 Results of ^{60}Co Gamma Irradiation Experiments. Crystal no. 2, which was of the type shown in Figure 3.10.1, was used for the gamma irradiation experiments. This crystal was given a total dose of 1.3×10^{18} gammas/cm^2 in three steps. Unlike the neutron-irradiated crystals, the gamma-irradiated crystals indicated some annealing at room temperatures (22); so the irradiation effects were not entirely cumulative. However, crystal no. 2 exhibited some interesting deviations from the simple g-r spectrum which were not observed in the neutron-irradiated crystals. Figure 4.6.1 shows the lifetime calculations from the g-r spectra. After the third irradiation (the crystal is now p-type), an extra hump appeared at some temperatures as shown in Figure 4.6.2. These humps change with temperature which excludes measurement errors. This type spectra cannot be explained by either the multilevel recombination theory or the ambipolar drift which results in a spectra of

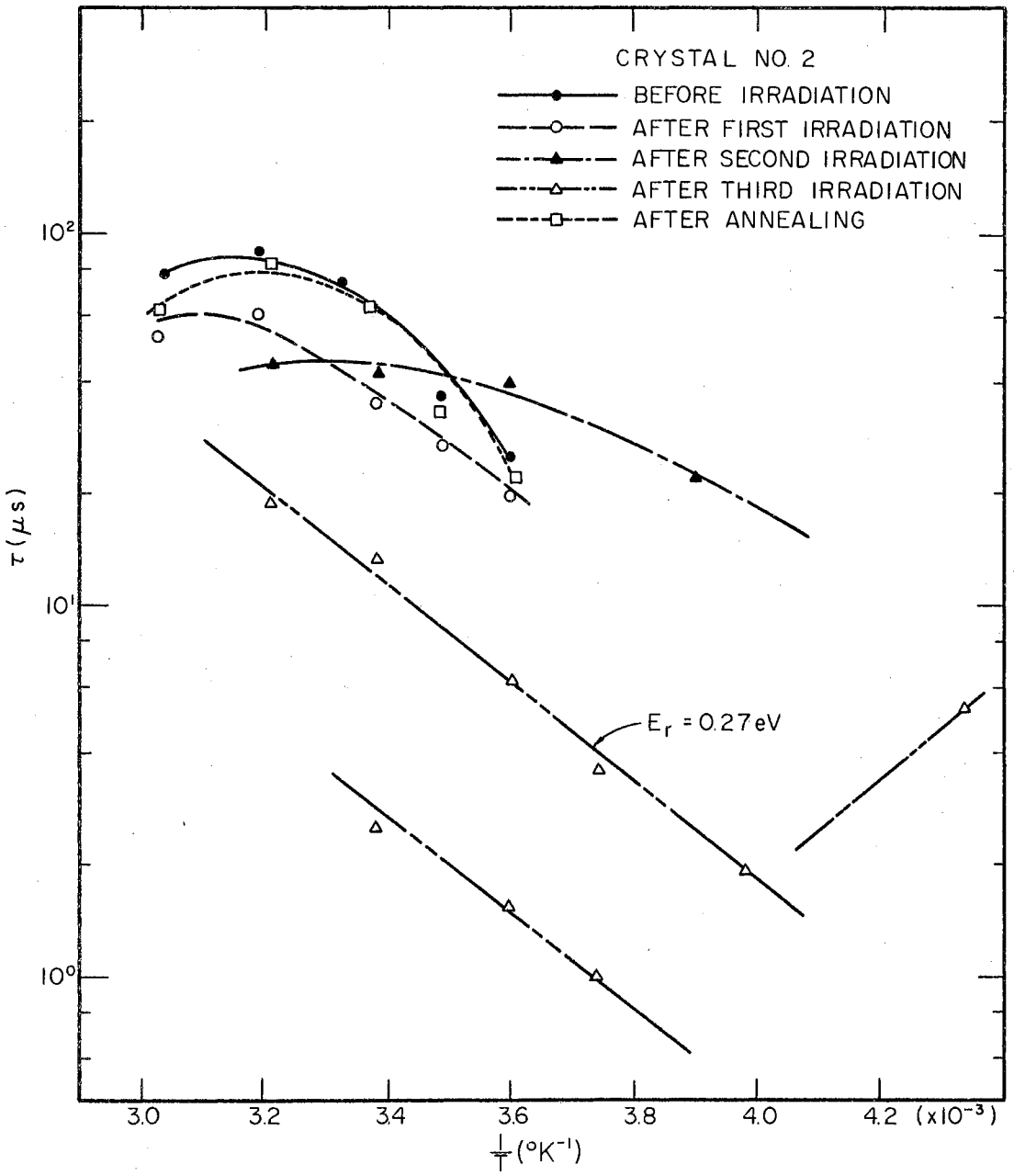

Figure 4.6.1. Lifetime Vs. 1/T for Crystal No. 2 Before Irradiation, After Irradiating With 4 x 10^{16}, 1.3 x 10^{17} and 1.4 x 10^{18} ^{60}Co Gammas per cm^2, and After Annealing at 350°C

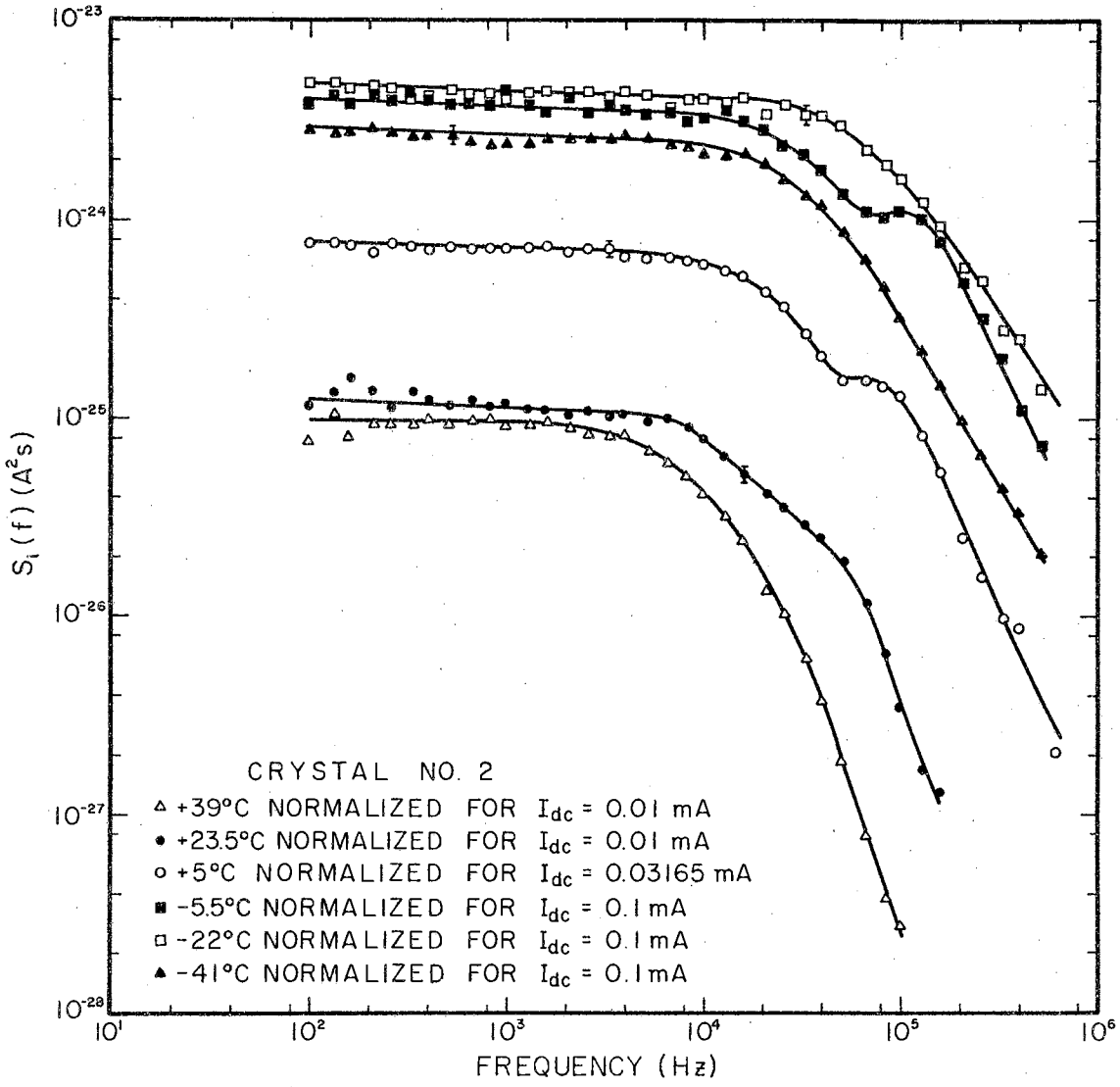

Figure 4.6.2. $S_i(f)$ Vs. Frequency for Crystal No. 2 After 1.4×10^{18} ^{60}Co Gammas per cm^2. Note That Some Curves are Normalized at Other Than 0.1 mA Crystal Current to Prevent Overlap

$$\left[\frac{\sin(\omega \tau_a/2)}{\omega \tau_a/2}\right]^2$$

for $\tau_a << \tau$. The multilevel theory gives rather smooth spectra, whereas these experiments show a resonant type effect. The peak of the ambipolar drift corresponding to $\omega \tau_a/2 = 3\pi/2$ is down 22 times from the maximum as compared to 4 times in our experimental results. These humps also occur in a very narrow temperature range. From the slope of the lifetimes in Figure 4.6.1, the depth of the recombination center can be calculated as 0.27 eV above the valence band. This is in good agreement with Curtis and Crawford (10) who found the recombination level 0.27 eV above the valence band after 9×10^{16} gammas/cm^2 on a 15 ohmcm antimony-doped germanium crystal (the $T^{3/2}$ term in the density of states has been neglected in the above calculations for the energy of the recombination center). The upward bend of the lifetime at low temperature is also in good agreement with Curtis-Crawford (10) and is introduced by the influence of a trapping level in addition to recombination centers.

Another interesting feature is seen on Figure 4.6.3 after the third irradiation. Here the curve has a definite upward trend at lower temperatures. It is also interesting to note that the points of deviation from a $1/(1 + \omega^2 \tau^2)$ type spectra occur at the three points about the local maximum of the n_r curve.

Figure 4.6.4 gives the results of the Hall effect measurements, where the conversion to p-type after the third irradiation is readily seen. The slope of the Hall curve at low temperatures indicates a recombination center at 0.29 eV which agrees well with the value found from the lifetime measurements. The resistivity data are given in Figure 4.6.5.

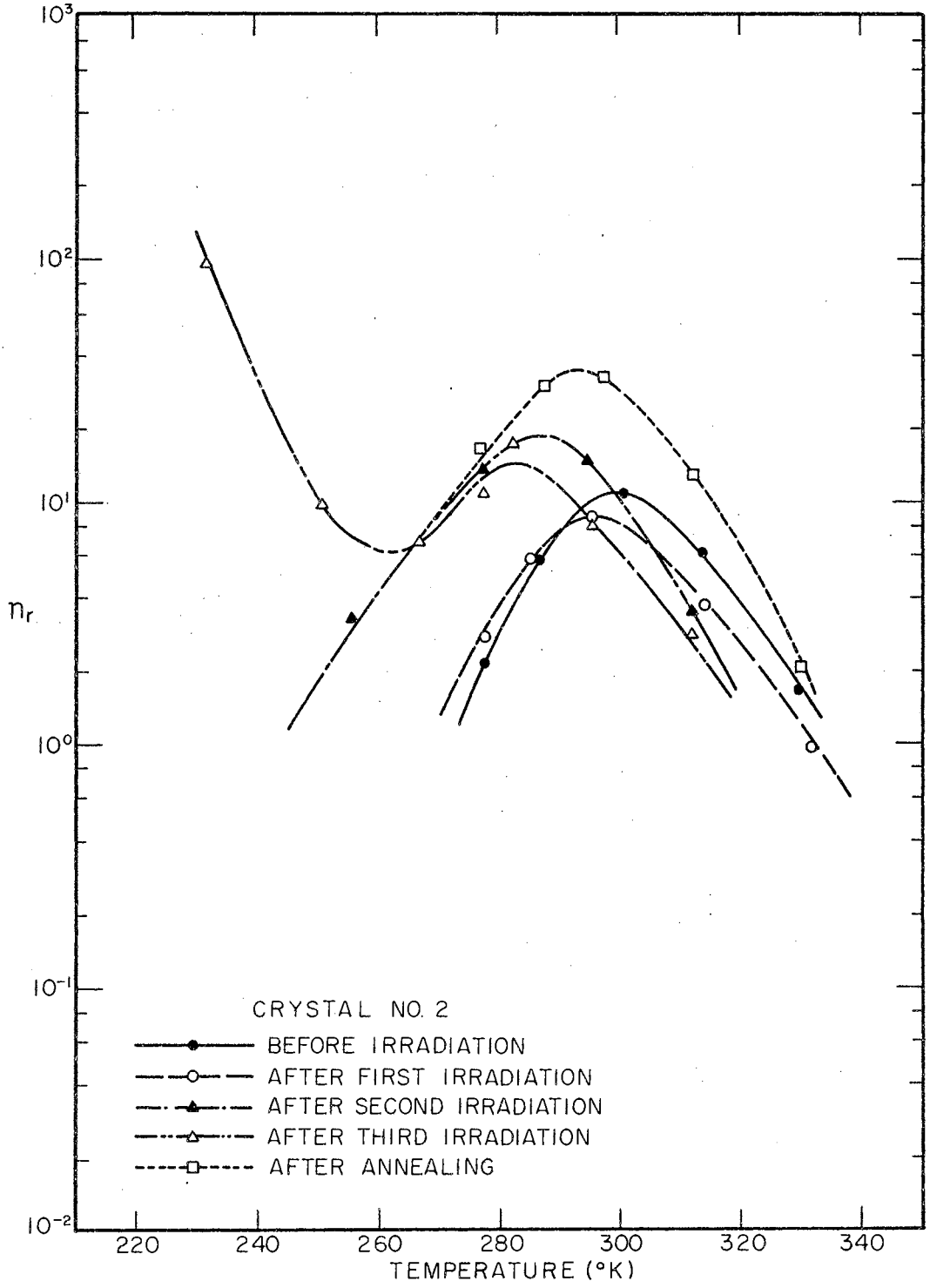

Figure 4.6.3. n_r Vs. T for Crystal No. 2. All Curves are Normalized to 0.1 mA Crystal Current

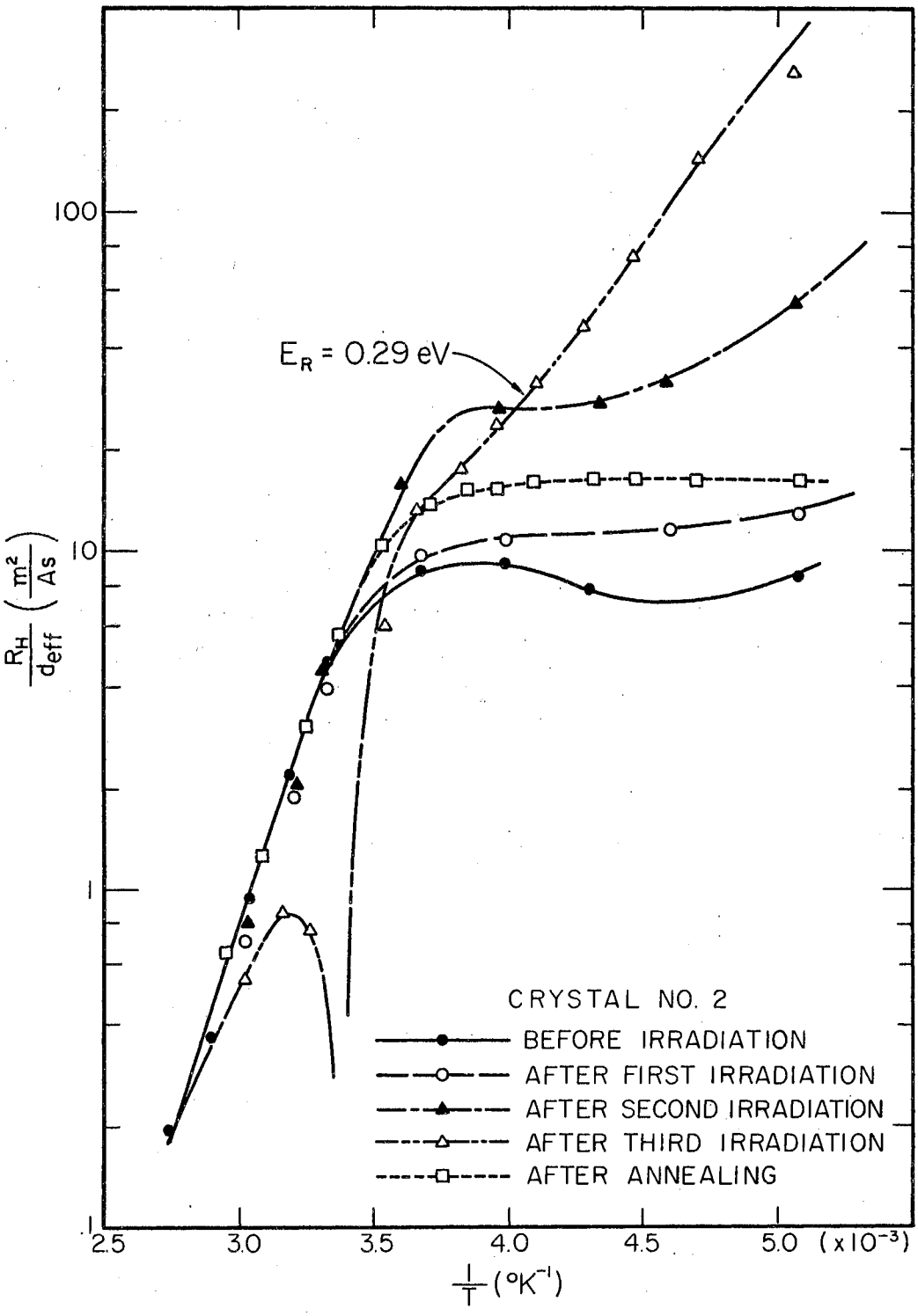

Figure 4.6.4. Hall Effect Vs. 1/T for Crystal No. 2. Compare With Figures 4.5.3, 4.5.4, and 4.5.10

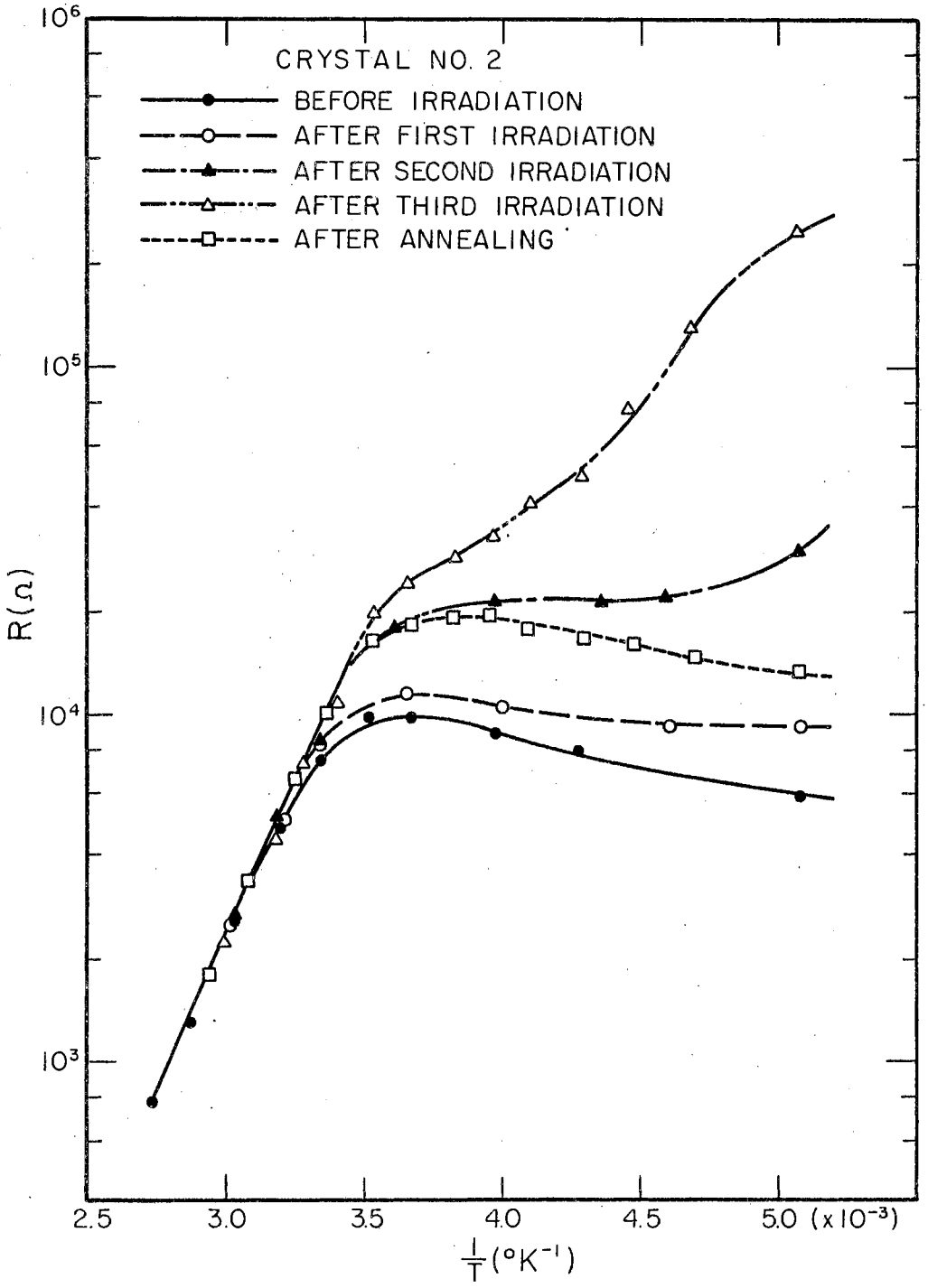

Figure 4.6.5. Resistance Vs. 1/T for Crystal No. 2 Before Irradiation, After Irradiating With 4×10^{16}, 1.3×10^{17} and 1.4×10^{18} ^{60}Co Gammas per cm^2, and After Annealing at 350°C

A compilation of the measurement results at room temperature is given in Table IV.

TABLE IV

SUMMARY OF RESULTS FROM CRYSTAL NO. 2

	$\tau(\mu s)$	f_c (KHz)	n_r (I_{DC} = 0.1 mA)	Effective Doping
Before Irrad.	130	2.1	12	n-type 4×10^{13}
After 4×10^{16} γ's/cm^2	65	45	9	n-type 3.1×10^{13}
After 1.3×10^{17} γ's/cm^2	58	37	12	n-type 1.3×10^{13}
After 1.4×10^{18} γ's/cm^2	36	12	6	p-type 2.7×10^{13}
After Annealing	144	2.4	30	n-type 2×10^{13}

Oen and Holmes (21) have calculated a theoretical value approximately 10^{-3}/cm^3 defects per incident ^{60}Co gamma ray; and Cleland, Crawford, and Holmes (8) have found experimentally 10^{-4}/cm^3 defects. The discrepancy is attributed to extensive relaxation of defects at room temperatures. We have 6.7×10^{13} electron removals per cm^3 (3.35×10^{13} vacancy-interstitial pairs) for a total irradiation of 1.4×10^{18} gammas/cm^2. This corresponds to 2.4×10^{-5} (cm^{-1}) defects per incident gamma ray. This discrepancy with the above findings is attributed to additional annealing at room temperature. A period of three months elapsed between the first irradiation and final measurement.

CHAPTER V

SUMMARY

5.1 Results and Conclusions. The experiments with neutron-irradiated germanium crystals have, in general, agreed with the theory except for the deviations found in crystal no. 9 after it became slightly p-type. Although only two crystals were used for the neutron irradiation portion of this thesis, generality can be claimed (except for the deviation just mentioned) as indicated in a previous paper by Bilger and McCarter (2).

Initial cutoff frequencies of 120 and 88 Hz have been obtained with crystals no. 9 and 10 which, to the knowledge of this author, is the lowest yet reported in the literature for g-r spectra. After irradiation by 14.7 MeV neutrons with a total dose of 2×10^{13} neutrons/cm^2, the cutoff frequency of crystal no. 9 changed to 85 KHz, an increase of 3 decades. By annealing crystal no. 9 to 550°C, the cutoff frequency was returned to 100 Hz. This procedure provides a reversible process for the crystal with respect to apparent doping, bulk lifetime, and g-r noise.

During this process, the noise ratio (n_r) varied over a range of 10^7. The picture of a simple g-r curve occurring from recombination at a single level is adequate to explain the n_r curves with the exception of the increase of n_r at lower temperatures after annealing.

The shift in lifetime and the corresponding change in doping as a

result of the neutron irradiation is in good agreement with the findings of others. This is the first time that a reversible g-r spectra and corresponding τ-change of many orders of magnitude have been accomplished with the same crystal.

The ^{60}Co gamma-irradiated crystal no. 2 did not undergo as large lifetime and apparent doping changes as the neutron-irradiated crystal, but some interesting results were obtained which are not explainable by today's theory of g-r spectra and ambipolar drift. Although ambipolar drift effects were shown to be in the picture, the ambipolar lifetime did not appreciably alter the spectra from a type of $1/(1 + \omega^2 \tau^2)$ at the initial and after annealing conditions when the bulk lifetime is the largest. The spectra were only altered after the crystal had changed to p-type. This suggests that some new theory must be developed in order to explain this phenomenon.

Crystal no. 2 was changed from n to p after an irradiation of 1.4×10^{18} gammas/cm^2 from a ^{60}Co source, and the lifetime decreased to 20 μs at 40°C. A subsequent annealing at 350°C returned the g-r spectra and (within a factor of 2) the apparent doping to the initial values. The irradiation defects from a ^{60}Co source are much easier annealed than those defects produced with fast neutrons (10).

5.2 Recommendation for Additional Study. The extension of the work on the gamma-irradiated crystal will be very helpful in developing an adequate theory which will explain the observed spectra after conversion to p-type. The nature of these spectra indicate that a type of resonance is occurring in the crystal over a very narrow temperature range. One possible explanation is a close coupling between several

levels in a multilevel recombination center.

The Fermi levels for the six temperatures of these g-r spectra are listed in Table V.

TABLE V

FERMI LEVELS OF CRYSTAL NO. 2 AFTER THIRD IRRADIATION

Temperature (°C)	E_f Above Valence Band (eV)
39	0.322
23.5	0.315
5	0.293
-5.5	0.28
-22	0.255
-41	0.23

The resonance points occur when the Fermi level is at or near 0.29 eV above the valence band. This is the energy of the recombination center as determined from the Hall effect data on Figure 4.6.4. The theoretical peak of a n_r spectrum with $N_A = 2.7 \times 10^{13}$ cm^{-3} occurs at 280°K according to theory. This corresponds to the local maximum observed for crystal no. 2 in the n_r curve. The new theory should explain the increase of τ and n_r at low temperatures as well as the resonance effects.

LIST OF REFERENCES

1. Bernamont, J. "Fluctuations de Potentiel aux Bornes d'un Conductor Métallique de faible Volume parcouru par un Courant." Annales de Physique. 7 (1937), 71.

2. Bilger, H. R. and E. R. McCarter. "Generation-Recombination Noise in Ge Single Crystals Under Fast-Neutron Irradiation." Journal of Applied Physics. 37 (1966), 1978.

3. Burgess, R. E. "Hole and Electron Fluctuations in a Semiconductor." Proceedings of the Physical Society (London). B68 (1955), 661.

4. _____. "The Statistics of Charge Carrier Fluctuations in Semiconductors." Proceedings of the Physical Society (London). B69 (1956), 100.

5. _____. "Fluctuations in the Number of Charge Carriers." Physica. 20 (1954), 1007.

6. _____. Fluctuation Phenomena in Solids. New York: Academic Press, 1965.

7. Cleland, J. W. and R. F. Bass. "Lattice-Defect Production in Ge by Photons and by Neutrons." Bulletin of American Physical Society. II (3) 8 (1963), 235.

8. Cleland, J. W., J. H. Crawford, Jr., and D. K. Holmes. "Effects of Gamma Irradiation on Germanium." Physical Review. 102 (1956), 722.

9. Curtis, O. L., Jr. and J. W. Cleland. "Monoenergetic Neutron Irradiation of Germanium." Journal of Applied Physics. 31 (1960), 423.

10. Curtis, O. L., Jr. and J. H. Crawford, Jr. "Radiation-Induced Recombination and Trapping Centers in Germanium." Physical Review. 124 (1961), 1731.

11. Davenport, W. B., Jr. and W. L. Root. Random Signals and Noise. New York: McGraw-Hill, 1958.

12. Glassford, G. M. Linear Analysis of Electronic Circuits. Reading, Massachusetts: Addison-Wesley, 1965.

13. Herzog, G. B. and A. van der Ziel. "Shot Noise in Germanium Single Crystals." Physical Review. 84 (1951), 1249.

14. Hill, J. E. and K. M. van Vliet. "Ambipolar Transport of Carrier Density Fluctuations in Germanium." Physica. 26 (1958), 709.

15. _____. "Generation Recombination Noise in Intrinsic and Near-Intrinsic Germanium Crystals." Journal of Applied Physics. 29 (1958), 177.

16. Kittel, C. Introduction to Solid State Physics. New York: Wiley, 1962.

17. Klaassen, F. M. "Generation-Recombination Noise in Semiconductors with Traps and Recombination Centers." Dissertation. Vrije Universiteit Te Amsterdam, 1961.

18. Lax, M. "Fluctuations from the Nonequilibrium Steady State." Reviews of Modern Physics. 32 (1960), 25.

19. _____. "Generalized Mobility Theory." Physical Review. 32 (1958), 1921.

20. Nyquist, H. "Thermal Agitation of Electric Charge in Conductors." Physical Review. 32 (1928), 110.

21. Oen, O. S. and D. K. Holmes. "Cross Sections for Atomic Displacements in Solids by Gamma Rays." Journal of Applied Physics. 30 (1959), 1289.

22. Saito, H., J. C. Pigg, and J. H. Crawford, Jr. "Annealing of ^{60}Co-Gamma-Irradiated Germanium." Physical Review. 144 (1966), 725.

23. Schottky, W. "Über spontane Stromschwankungen in verschiedenen Elektrizitätsleitern." Annalen der Physik. 57 (1918), 541.

24. Shockley, W. Electrons and Holes in Semiconductors. New Jersey: Van Nostrand, 1950.

25. Shockley, W. and W. T. Read, Jr. "Statistics of the Recombinations of Holes and Electrons." Physical Review. 87 (1952), 835.

26. van der Ziel, A. Fluctuations Phenomena in Semiconductors. London: Butterworths Scientific Publications, 1959, Chapter 4.

27. _____. Noise. New York: Prentice-Hall, 1954.

28. van Roosbroeck, W. and W. Shockley. "Photon-Radiative Recombination of Electrons and Holes in Germanium." Physical Review. 94 (1954), 1558.

29. van Vliet, K. M. "Irreversible Thermodynamics and Carrier Density Fluctuations in Semiconductors." Physical Review. 110 (1958), 50.

30. _____. "Noise in Semiconductors and Photocondcutors." Proceedings of the I.R.E. 46 (1958), 1004.

31. _____. "Current Fluctuations in Semiconductors and Photoconductors." Dissertation. Vrije Universiteit Te Amsterdam, April, 1956.

32. van Vliet, K. M. and J. Blok. "Electronic Noise in Semiconductors." Physica. 22 (1956), 231.

33. van Wijngaarden, J. G., K. M. van Vliet, and C. J. van Leeuwen. "Low Frequency Noise in Electron Tubes." Physica. 18 (1952), 689.

34. Williams, N. H. and E. W. Thatcher. "On Thermal Electronic Agitation in Conductors." Physical Review. 40 (1932), 121.

APPENDIX A

ERROR ANALYSIS

A.1 Theoretical Investigation. The output voltage of the narrow band (6.75 Hz) wave analyzer has fluctuations which are of the order of the amplitude of the desired reading itself. In order to obtain a reading with an expected error of only 1.36 percent, the output voltage is integrated (using operational amplifiers) for 100 seconds and subsequently read out on a precision VTVM. This has the following advantages over an RC integrator:

a. Only one time constant of waiting is needed.

b. The output does not fluctuate while reading.

c. (To be shown) the relative error is smaller than with an RC integrator of the same time constant.

Using the methods of Davenport and Root (11) and van der Ziel (27), a narrow band noise voltage of width B centered about a frequency f_c (narrow band means $B < f_c/5$) can be represented by the following expressions:

$$x(t) = V(t) \cos [\omega_c t + \phi(t)] \qquad (A.1.1)$$

and

$$x(t) = x_c(t) \cos \omega_c t - x_s(t) \sin \omega_c t \qquad (A.1.2)$$

where

$$V(t) = [x_c^2(t) + x_s^2(t)]^{1/2} \qquad (A.1.3)$$

From Equation A.1.3 it is obvious that $V(t) \geq 0$. The wave analyzer full-wave-rectifies x(t) and filters the result so that the envelope V(t) is retained, and the carrier frequency and its components are removed. It can easily be shown that the normalized frequency response of an integrator is

$$h(f) = \frac{\sin 2\pi fT}{2\pi fT} \qquad (A.1.4)$$

where T is the integration time. Following Sec. 13 of van der Ziel (27), the expected error ($\alpha^{1/2}$) is given by

$$\alpha = \frac{1}{8BT} \qquad (A.1.5)$$

This is the same as the expected error for an RC integrator with the same time constant, but one must wait an infinite time (in practice: several time constants) before achieving this error with an RC integrator; so, in only one time period (T), an integrator has much less error than an RC integrator.

To verify Equation A.1.5, 100 measurements were made of a noise due to a 10 KΩ resistor attached at the input of the amplifier and 600 μA flowing through the noise diode. From these measurements a mean of 174.4 (arbitrary units) and a standard deviation of 2.67 was calculated. This results in a relative standard error ($\sqrt{\alpha} = \sigma/\bar{x}$) of 1.53 percent. Applying the measured RMS bandwidth of 6.75 Hz and the integration time of 100 seconds to Equation A.1.5 results in a relative error of 1.36 percent, which is in good agreement with the measured results. The experimental data, a Gaussian with the same mean and

variance, and the theoretical Gaussian is shown in Figure A.2.1. Since these 100 measurements were taken consecutively (total time of experiment $>10^4$ seconds), Figure A.2.1 demonstrates also absence of drift in the whole noise spectrometer.

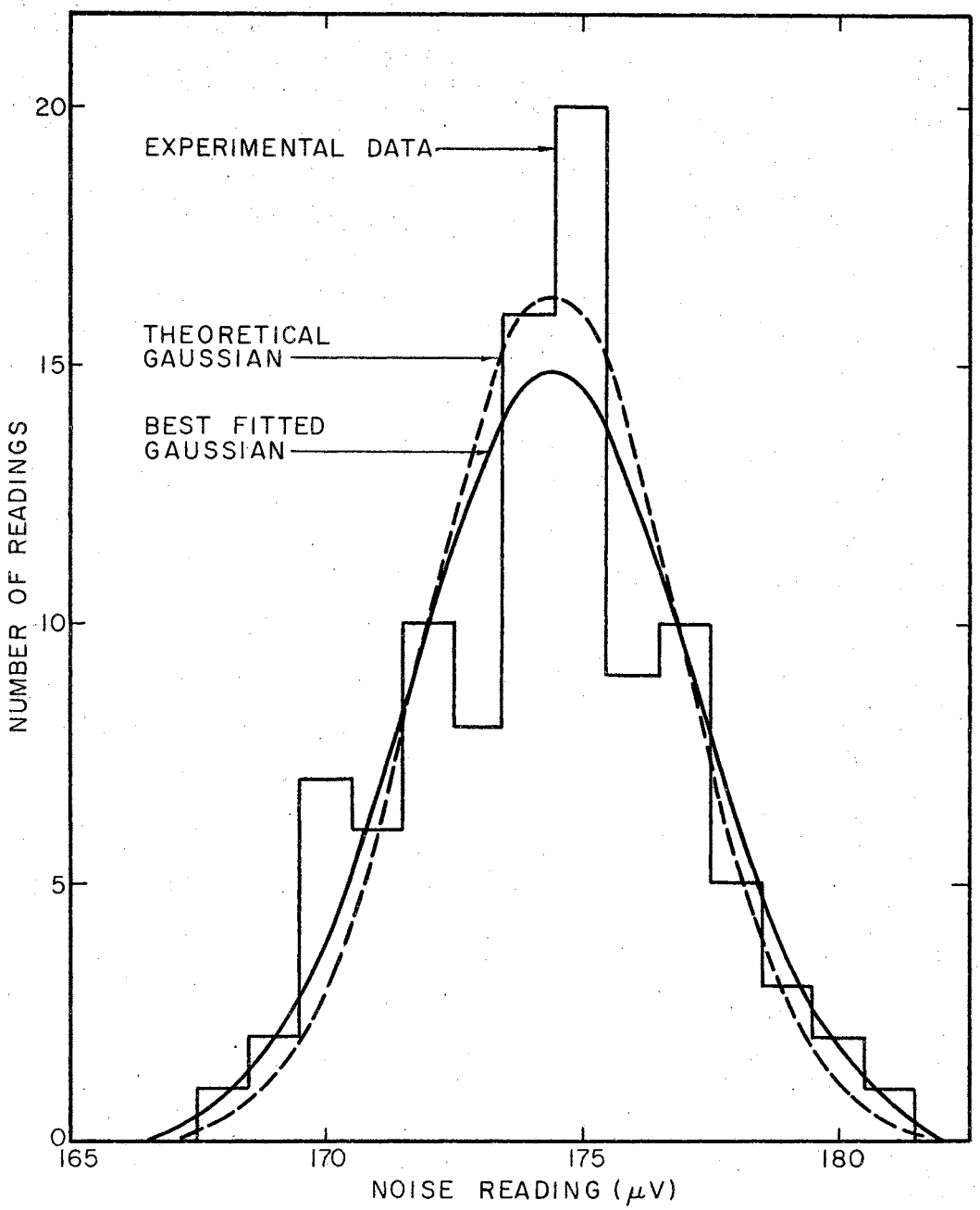

Figure A.2.1. Experimental Data for 100 Noise Readings, A Gaussian With the Same Mean and Variance as the Experimental Data, and the Theoretical Gaussian

VITA

Ed Raymond McCarter

Candidate for the Degree of

Doctor of Philosophy

Thesis: A REVERSIBLE NUCLEAR RADIATION APPROACH TO GENERATION-RECOMBINATION NOISE STUDIES IN GE-SINGLE CRYSTALS

Major Field: Electrical Engineering

Biographical:

Personal Data: Born at Muskogee, Oklahoma, December 16, 1926, the son of Clyde and Margaret McCarter.

Education: Attended through grade 8 in Muskogee, Oklahoma; grades 9 through 11 were attended at Stillwater, Oklahoma; graduated from Field Kindley High School, Coffeyville, Kansas, in 1944; received the Bachelor of Science degree in Electrical Engineering from Oklahoma State University in January, 1951; received the Master of Science degree in Electrical Engineering from Oklahoma State University in May, 1965; completed requirements for the Doctor of Philosophy degree in May, 1967.

Professional Experience: Served in the United States Navy from November, 1944, to October, 1947. Employed by the Jersey Production Research Company of Tulsa, Oklahoma, from January, 1951, to September, 1964. Held the position of Senior Research Engineer and is presently on leave of absence while continuing education.

Professional Organizations: Registered Professional Engineer, Oklahoma; member of the Institute of Electrical and Electronics Engineers, Phi Kappa Phi, Sigma Tau, Eta Kappa Nu, and Pi Mu Epsilon